Reprinted from MONTHLY WEATHER REVIEW, Vol. 120, No. 1, January 1992
American Meteorological Society

Three-Dimensional Mean and Turbulence Structure of a Coastal Front Influenced by the Gulf Stream

TEDDY R. HOLT

Department of Meteorology, Naval Postgraduate School, Monterey, California

SETHU RAMAN

Department of Marine, Earth, and Atmospheric Sciences, North Carolina State University, Raleigh, North Carolina

(Manuscript received 26 December 1990, in final form 13 June 1991)

ABSTRACT

The interaction of oceanic fronts in the vicinity of the Gulf Stream with an atmospheric coastal front during the Genesis of Atlantic Lows Experiment (GALE) is examined using aircraft, satellite, and ship data. The nearshore, midshelf, and Gulf Stream oceanic fronts are readily discernible from low-level aircraft radiometer and satellite imagery data. The three-dimensional (3D) structure of the coastal front is extensively mapped by low-level aircraft transects through the frontal boundary.

Results confirm the existence of the coastal front as a very shallow (depth less than 200 m), spatially inhomogeneous, undulating material surface. Aircraft observations from 2000 to 2200 UTC (late afternoon local time) show a surface location of the coastal front that is aligned over the Gulf Stream oceanic front under conditions of very weak (2 m s^{-1}) onshore flow, but is observed to migrate shoreward for stronger onshore flow.

Ahead of the front in the warm air, the marine atmospheric boundary layer is characterized as well mixed with broken cumulus and stratocumulus cloud bases observed near 500 m, and tops varying from 1300 to 1900 m. The dominant scale of turbulent eddies is observed to be on the order of the boundary-layer depth. Conditional sampling statistics point to a strong direct circulation ahead of the front dominated by intense, narrow, warm updrafts, and broader, less intense, cool downdrafts.

Behind the coastal front in the cold air, visibility is much reduced by low-level fractus and layered stratocumulus clouds. The shallow subcloud layer is observed to be generally moister and more statically stable than ahead of the front. It is also characterized by an indirect circulation with more prevalent cool updrafts and warm downdrafts, particularly for the near–cloud-base region.

However, behind the front there exists a strong thermodynamic coupling of atmosphere and ocean as evidenced by the distinctly different atmospheric regimes present over the oceanic nearshore and midshelf front regions. Over the nearshore region, the horizontal wind structure is dominated by 100-m waves imbedded in a weaker 1–2-km circulation. Warm updrafts are observed over the nearshore waters, but the smaller air–sea temperature difference effectively limits large temperature perturbations. Hence, much smaller sensible heat flux is evident over the nearshore region as compared to the oceanic midshelf region. Over the midshelf region, turbulent eddies on the scale of 1.5 times the depth of the front (120 m) are solely responsible for the larger positive heat flux. The transition zone of the coastal front aloft near 150 m is remarkably confined to just the oceanic nearshore shelf, located between the nearshore waters and the midshelf region.

The frontal surface itself is observed to play an important role in the 3D atmospheric circulation in the vicinity of the front. The front causes a decoupling of the region just above the frontal surface by inhibiting the vertical transfer of fluxes from the surface. Cospectra for regions just above the front show no contributions from smaller waves generated by near-surface processes (on the order of 100–500 m) that are evident just ahead of the front. This suggests a decoupling due to the frontal boundary. Associated with this decoupling and the subsequent stabilization of the region above the front is the occurrence of buoyancy waves. These waves of wavelength approximately 840 m are believed to be a result of penetrating thermals and/or instabilities present along the frontal surface.

1. Introduction

For the past 40 years meteorologists have sought to document the features associated with coastal front formation and development. Knowledge of this very shallow baroclinic zone has progressed from the work of Carson (1950), who observed wintertime stratus off the east coast of the United States associated with the Gulf Stream (GS) front, to the more recent works of Bosart (1975), Marks and Austin (1979), Ballentine (1980), and Nielsen and Neilley (1990), who documented relevant synoptics, dynamics, and precipitation structure of New England coastal-front formation.

The importance of the coastal front in providing an

Corresponding author address: Dr. Teddy R. Holt, Department of Meteorology, Naval Postgraduate School, Monterey, CA 93943-5100.

environment conducive to subsequent cyclogenesis is well documented (Bosart and Lin 1984). In the evolution of 18 major East Coast cyclones, Kocin and Uccellini (1984) noted that coastal fronts were present for 13 storms. Our knowledge of the coastal front as an important source of low-level moisture and positive vorticity aiding cyclogenesis is well specified, as is the variety of physical mechanisms identified as important contributors to coastal frontogenesis. Among them are the land–sea temperature contrast, coastal configuration, differential surface roughness, and differential diabatic heating (Bosart 1975).

The purpose of this paper is to document the 3D atmospheric mean and turbulence structure of a shallow coastal front observed offshore of North Carolina on 12 March 1986 during the Genesis of Atlantic Lows Experiment (GALE). The goal is to understand the interaction between the dynamics of the coastal front and the underlying GS sea surface temperature (SST) discontinuity. The relationship between atmospheric fronts that form in response to SST discontinuities (such as at the north wall of the GS) and coastal fronts, which form in the same vicinity, but often due to a variety of different physical mechanisms, is not well understood (Warner et al. 1990). Up until now, a clear delineation of the dynamics of the two fronts has not been attempted.

Recent studies have examined the dynamics of the marine atmospheric boundary layer (MABL) due only to SST discontinuities. Rogers (1989) and Khalsa and Greenhut (1989) considered the MABL structure in the vicinity of oceanic fronts or SST discontinuities during the 1986 Frontal Air–Sea Interaction Experiment (FASINEX). Results from FASINEX, which are considered valid for open-ocean temperature fronts, have contrasted the vertical structure of the MABL on the warm side of the oceanic front with that of the cold side. Herbster (1990) emphasized that the presence of a SST front can produce rapid modifications to MABL circulation. Khalsa and Greenhut (1989) provided evidence for secondary circulation in the vicinity of the SST front, emphasizing that surface divergence and subsidence caused by the strong, frontally induced pressure gradient over the warm water resulted in a sinking dry-air region. A related numerical study by Wai and Stage (1989) emphasized a similar MABL circulation near a GS oceanic front. However, each of these studies considered only the MABL as related to a SST front and did not specifically address the relationship, structure, and dynamics of the oceanic front and the coastal front.

Knowledge of the smaller-scale (mesogamma-scale) structure of fronts has been limited by the lack of routinely available observations. Previous studies of the coastal front and its dynamics have pertained to the mean structure, or model-generated forecasts of mean and turbulent structure, because turbulence data of this elusive phenomenon were not available. GALE, conducted off the Carolinas from 15 January to 15 March 1986, provided a high temporal and high spatial resolution dataset capable of resolving coastal frontogenesis processes (see Raman and Riordan 1988, for details on the GALE field project). An extensive array of special measurement platforms, including MABL research aircraft, were utilized during GALE. The aircraft considered in the 12 March study made several low-level passes through the coastal front. In section 2, we consider the synoptic setting and basic experiment design including data collection and analysis for 12 March. Section 3 details the location, characteristics, and mean structure of the coastal front in relation to the oceanic front. In section 4, turbulence structure is considered in detail. Spectra and cospectra are utilized to understand the important scales of motion. Transects through the coastal front are examined using conditional sampling to investigate the existence of convective thermals or waves in and along the front. A discussion and conclusions are given in section 5.

2. The setting

a. Synoptics

The synoptic conditions on 12 March 1986 were favorable for coastal frontogenesis offshore of North and South Carolina. The 1200 UTC National Meteorological Center (NMC) surface analysis (Fig. 1a) indicated a cold 1032-mb anticyclone in the eastern James Bay (50°N, 77.5°W) well north of the GALE area. The southern region of this anticyclonic surface flow reached into North and South Carolina with a cool wedge of air dammed from the North Carolina–South Carolina border westward to the Appalachian Mountains. The presence of the cold anticyclone to the north provided "classic" north-northeasterly flow along the coast, conducive for coastal frontogenesis (Bosart et al. 1972).

A cold front that pushed through earlier (0000 UTC 12 March) was situated west-northwest to east-southeast through western North Carolina and northern South Carolina (Fig. 1a) and showed little movement for the following 12 h (Figs. 1b,c). Upper-level flow (500 mb) at 1200 UTC 12 March and 0000 UTC 13 March (Figs. 2a,b) indicated a building ridge in the Great Lakes region upstream of the cold surface anticyclone. Such a location provided upper-level support for the maintenance of the surface anticyclone through 1200 UTC 13 March.

It should be noted that at 1200 UTC 12 March near-surface flow up to an altitude of approximately 400 m for regions offshore of North and South Carolina was predominantly north-northwesterly (offshore) (Fig. 3) instead of relatively warm, moist onshore flow typically associated with the coastal front. This suggests that, for this area, the front had not yet developed at 1200 UTC (see section 3).

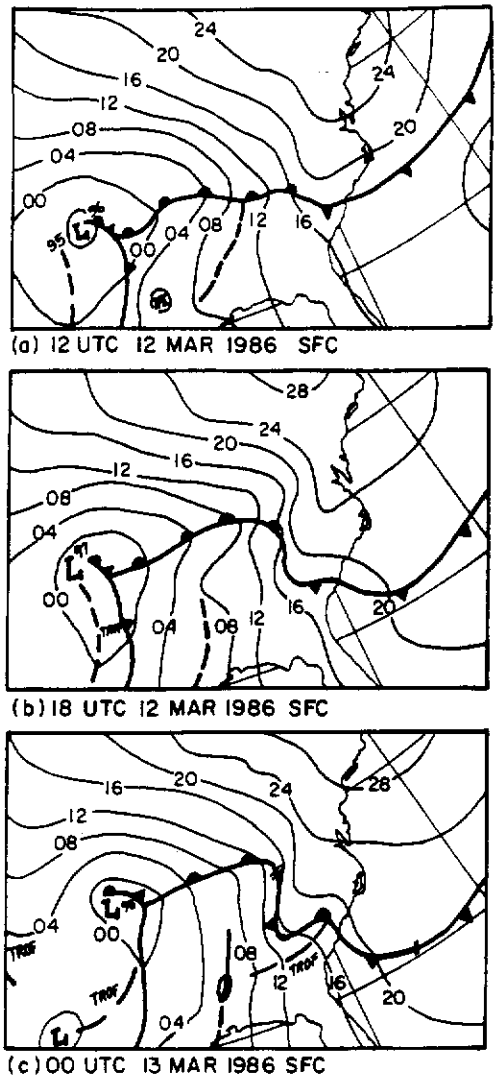

FIG. 1. NMC surface analysis for (a) 1200 UTC 12 March 1986, (b) 1800 UTC 12 March 1986, and (c) 0000 UTC 13 March 1986. The isobar interval is 4 mb.

b. *Experiment design*

Quantitative observations of the MABL on 12 March were obtained from a variety of platforms. The primary data source was the National Center for Atmospheric Research (NCAR) King Air research aircraft. An additional aircraft operating in the area, the NCAR Electra, also provided supporting observations. Figure 4 shows the flight tracks of the two aircraft offshore of North Carolina along with the high-resolution (2.5 km) sea surface temperature (SST) field obtained from the *NOAA-9* satellite. The Electra mission (1200–1900 UTC) was designed to examine the vertical structure of the mean and turbulent MABL for prestorm conditions of an offshore cyclogenesis case. To accomplish this task, the Electra flew four vertical "stacks" at strategic locations offshore. Each stack consisted of four to six level horizontal legs of length 30–32 km at various altitudes in the MABL. The first stack (EA: centered near 33.8°N, 76.8°W) was located west of the GS over the cooler nearshore waters (SST = 18°C). The second stack (EB: 34.1°N, 75.9°W) was located near the western edge of the GS (SST = 24°C), and the last two stacks (EC and ED: 34.0°N, 73.5°W) were located over the GS farther east (SST = 20°–21°C). Only three of these stacks are considered in this study (EA, EB, and EC in Fig. 4). The fourth stack (ED) was approximately 75–100 km east of stack EC and showed little difference in vertical structure. Table 1 provides information for the various levels of each stack. In addition, vertical ascent or descent profiles were flown at each stack to provide mean vertical structure.

While the primary emphasis of the Electra mission was to examine the vertical MABL structure, the King Air mission (2000–2200 UTC) was designed to provide

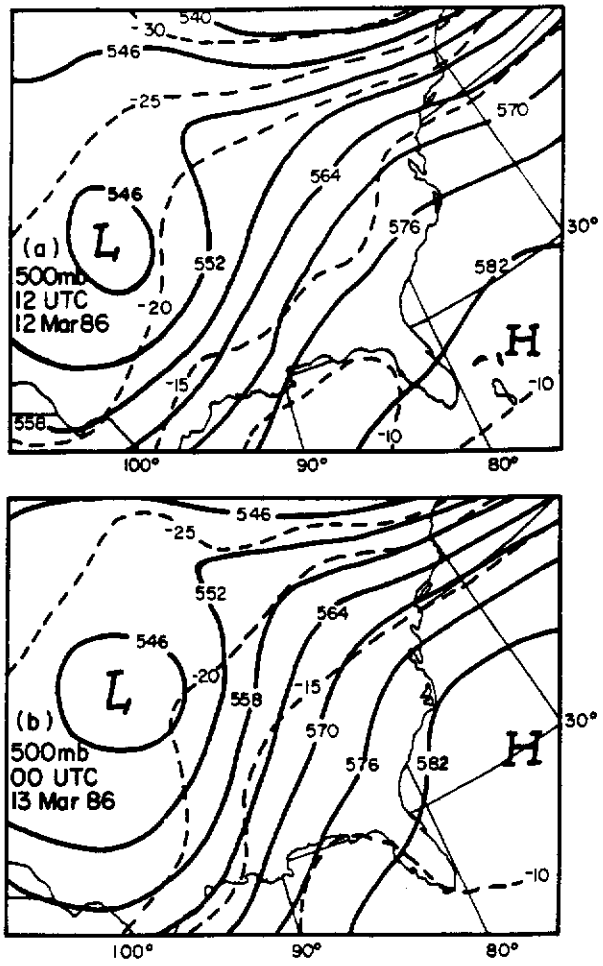

FIG. 2. NMC 500-mb analysis of height (dam, solid lines) and temperature (°C, dashed lines) for (a) 1200 UTC 12 March 1986 and (b) 0000 UTC 13 March 1986. Contour intervals are 6 dam and 5°C.

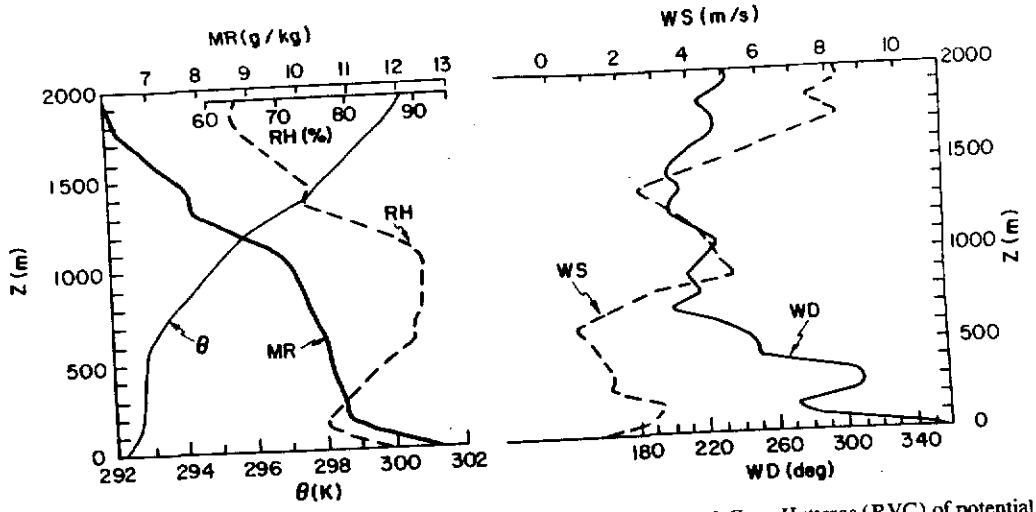

FIG. 3. The 1200 UTC 12 March 1986 CLASS sounding at the research vessel *Cape Hatteras* (RVC) of potential temperature θ, mixing ratio MR, relative humidity RH, wind speed WS, and direction WD.

extensive mapping of the horizontal and low-level vertical structure of the coastal front. The King Air flight track was almost exclusively limited to low-level horizontal transects in the coastal front region, with the exception of the vertical stacks at *A* and *E* (legs 20 to 25 km in length) (see Table 1 for details).

Two low-level horizontal transects of approximately 85 km each were flown between points *A* and *B*. The first transect from *A* to *B* (2002–2020 UTC) at an altitude of approximately 30 m was designed to give low-level turbulence structure across the coastal front, as well as provide a fix on the location of the front. The return transect from *B* to *A* (2022–2036 UTC) at approximately 148 m was designed to intercept the front aloft and give turbulence structure across the front near the frontal interface. In addition, the vertical slope of the frontal boundary is estimated from the position of the front aloft in relation to the near-surface (30-m) position.

After a four-level stack at *A* (2038–2102 UTC), a second transect from *A* toward *B* at 30 m was performed. The mission plan was to use the position of the coastal front determined from the previous *AB* transect (designated as point *C*: 34.62°N, 75.53°W) and fly from *A* to *C* at 30-m altitude, then proceed southwestward with a fixed aircraft heading of 230° to point *D* (34.3°N, 76.0°W) to roughly parallel the SST isotherms and hopefully parallel the coastal front. At point *D* the King Air would turn south (toward point *E*) to intercept the research vessel *Cape Hatteras* (RVC) (on station at 33.9°N, 76.0°W). At point *E* (33.8°N, 76.0°W) on the warm side of the front, the King Air performed a vertical stack with RVC located at the northeasterly end of the pattern.

In addition to aircraft observations, supporting observations of mean vertical soundings from the Cross-chain Loran Atmospheric Sounding System (CLASS) aboard the RVC at 1200, 1500, 1800, and 2100 UTC 12 March were also obtained.

c. *Aircraft turbulence data and analysis*

A description of the instrumentation on board the King Air and the Electra is discussed in detail elsewhere (see LeMone and Pennell 1980; Lenschow and Spyers-

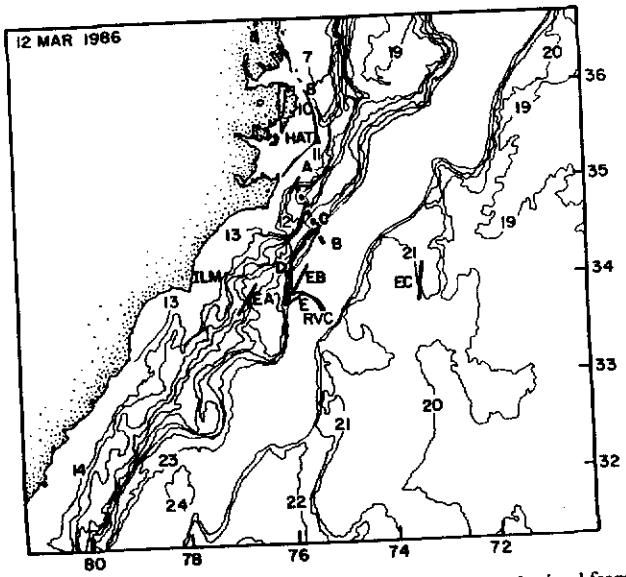

FIG. 4. High-resolution sea surface temperature field obtained from *NOAA-9* satellite imagery. Contour interval is 1°C. Low-level King Air aircraft flight tracks are given by dashed lines. Solid lines indicate regions of King Air (A, E) and Electra (EA, EB, EC) vertical aircraft stacks.

TABLE 1. 12 March 1986 Aircraft stacks.

Stack	Latitude (°N)	Longitude (°W)	Time (UTC)	z (m)	Heading (deg)
EA	33.83	76.76	1354:01–1359:00	37	215
			1403:01–1408:00	108	37
			1412:01–1417:00	182	213
			1420:31–1425:30	310	37
EB	34.06	75.87	1449:01–1454:00	40	41
			1458:01–1503:00	116	215
			1507:01–1512:00	185	45
			1516:01–1521:00	316	215
EC	33.97	73.50	1606:01–1611:00	37	10
			1615:01–1620:00	115	185
			1624:30–1629:30	178	18
			1634:10–1639:10	678	190
A	35.02	75.72	2038:10–2043:10	30	36
			2045:00–2049:10	86	215
			2051:00–2055:30	157	38
			2057:15–2101:45	275	216
E	33.80	76.00	2147:01–2151:30	28	231
			2153:31–2158:30	88	56
			2202:01–2207:00	433	230
			2209:30–2214:10	872	52
			2217:01–2222:00	1432	230
			2228:01–2231:00	1737	02

Duran 1986). Only a brief discussion of the aircraft turbulence data and analysis utilized in this study is given here.

To consider turbulence characteristics of the boundary layer in the vicinity of the coastal front, conditioning of the raw aircraft data was performed to remove contributions from larger nonturbulent events. Aircraft turbulence data were recorded at 50 samples per second. Postprocessing of all data then involved digital filtering with four-pole low-pass Butterworth filters with a 10-Hz cutoff frequency (corresponding to a response function at 10 Hz of 0.707). Data were then interpolated to 20 samples per second. A compound running mean subtraction filter that effectively removes low frequencies ($\lambda > 10$ km) was then employed. The transfer function $T(f)$ of the compound running mean is given as:

$$T(f) = [1 - \sin(\pi f t_1)\sin(\pi f t_2)(\pi^2 f^2 t_1 t_2)^{-1}]^2 \quad (1)$$

where f is frequency, and t_1 and t_2 are the length (s) of the primary and secondary running means, respectively. This filter was chosen because the transfer function is better behaved than that of a simple running mean. For example, for 20-Hz King Air data, with an aircraft speed of approximately 75 m s^{-1}, running mean lengths $t_1 = 51.4$ s and $t_2 = 0.7t_1 = 36.0$ s, result in 90% reduction of spectral power for $\lambda = 10$ km with little effect at smaller wavelengths.

Calibration of the 20-Hz Lyman-α humidity data was achieved using the method of Lind and Shaw (1991) in which a linear regression of Lyman-α data on 1-Hz hygrometer data was performed.

Values of SST determined from the downward-viewing radiometer were not corrected for reflected sky radiation or atmospheric absorption. Downwelled infrared radiation reflected from the ocean surface is generally only important in broken cloud conditions, especially cumulus clouds, for which the magnitude of the error in SST can vary up to 0.5°C (Liu and Katsaros 1984). Across the oceanic front during FASINEX, Herbster (1990) indicated that SST errors can also vary up to 0.5°C due to atmospheric absorption. While these errors in SST can be significant, it should be noted that the relative sensitivity of the radiometer is quite good. Thus, in this study for the purpose of positioning the location of the SST front, corrections to SST values obtained from the downward-viewing radiometer will not significantly affect the determination of the frontal location.

3. Description of the coastal-front environment

a. Frontal location

Figure 5 shows time series traces of SST, potential temperature θ, mixing ratio MR, wind direction WD, wind speed WS, and vertical velocity w for the 30-m transect from A to B, and the return 148-m transect from B to A. Four separate regions (designated as NS, NSS, MS, and GS) are indicated in Fig. 5 as derived from the SST field (Fig. 5a). Region NS indicates the nearshore waters where the SST ranged from 12° to 17°C. Region NSS indicates the nearshore shelf characterized as the approximately constant (18°C) SST region between the oceanic nearshore and midshelf fronts. Region MS delineates the midshelf characterized as the approximately constant (20°C) SST region between the midshelf front and the GS front. The SST of the GS region is approximately 24°C.

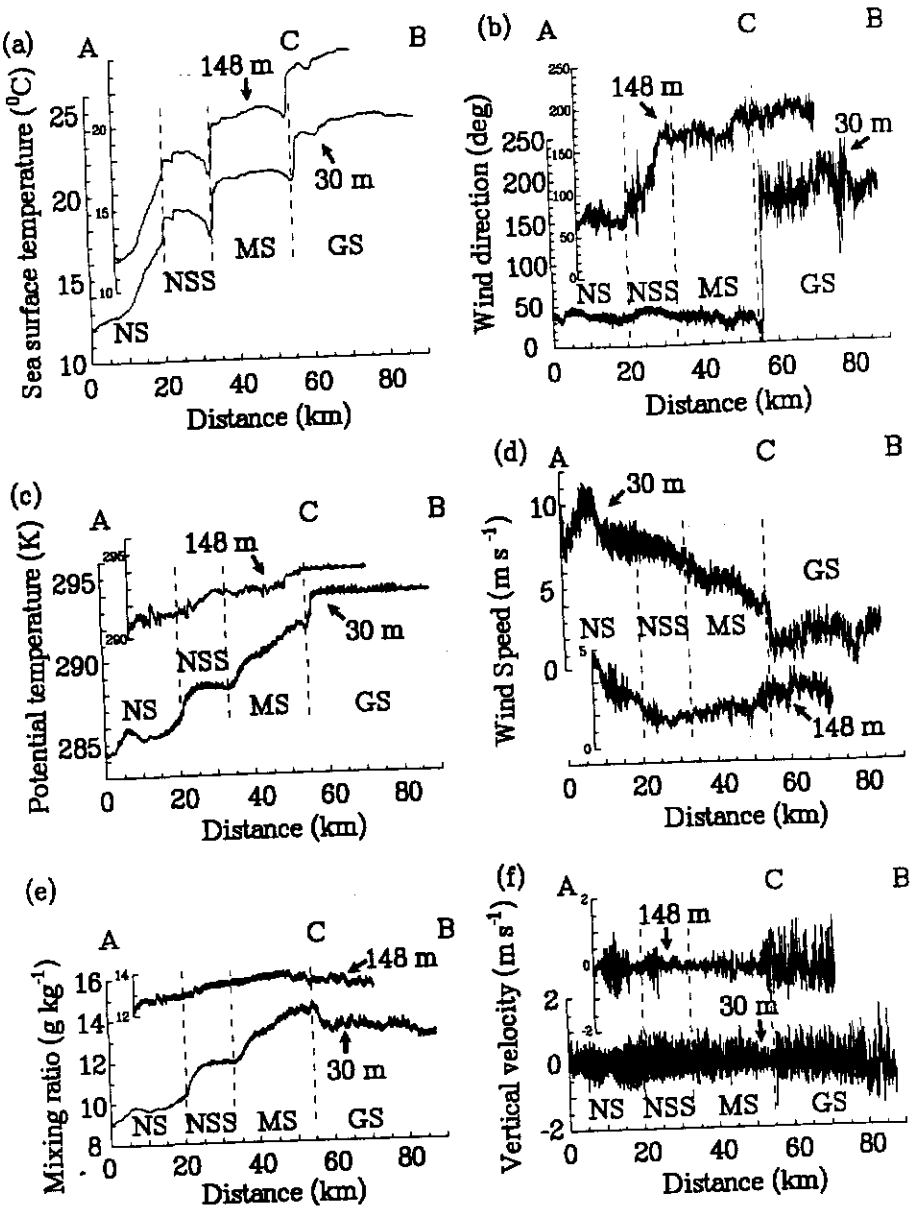

FIG. 5. King Air time series traces from A to B at 30 m and the return transect from B to A at 148 m of (a) sea surface temperature, (b) wind direction, (c) potential temperature, (d) wind speed, (e) mixing ratio, and (f) vertical velocity. Regions indicated as nearshore (NS), nearshore shelf (NSS), midshelf (MS), and Gulf Stream (GS) are determined from the sea surface temperature transect. The three dashed vertical lines represent the nearshore front, midshelf front, and Gulf Stream front.

The coastal front is most easily distinguished in the WD trace (Fig. 5b). Behind the front at 30 m the winds are nearly unidirectional from 40°. The winds shift rapidly on the warm side of the front to 160°–200°. Note that the coastal front boundary at 30-m altitude (as determined from θ and WD) is aligned over the GS front.

From the 148-m transect the location of the frontal boundary is not as easily pinpointed. From the WD trace (Fig. 5b) the winds vary only from 160° to 200° over the GS and MS regions. The transition zone at 148 m from the warmer, southerly flow to the cooler, northerly flow occurs over roughly a 10-km distance over NSS. Thus, the slope of the frontal boundary along transect AB appears steeper near the surface than at a height of 148 m. Indeed, if the coastal front is "tied" to the western edge of the GS at this time, then the boundary is vertical at point C (as indicated in Fig. 7).

The time series traces at 30 m from C to D (roughly parallel to the coastal front along the 20°C SST iso-

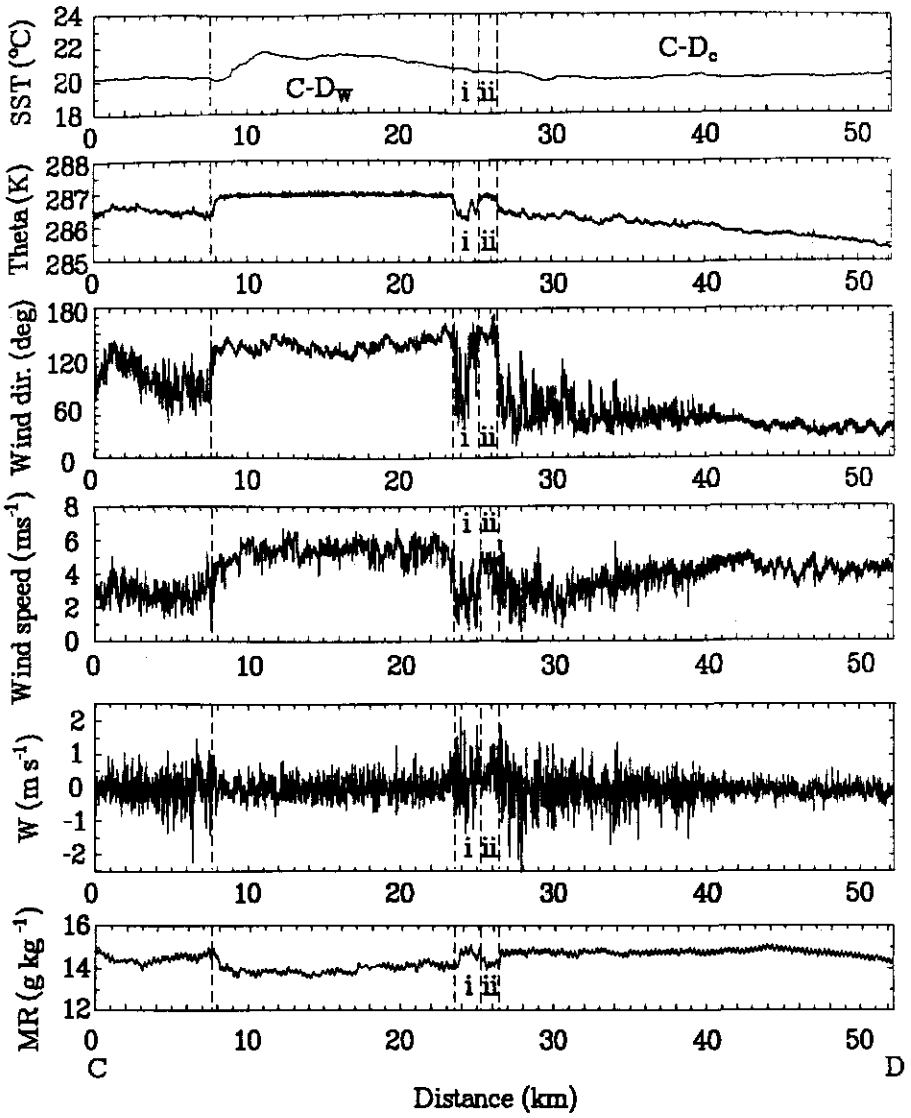

FIG. 6. King Air time series traces as given in Fig. 5, but for the 30-m transect from C to D. Regions (i) and (ii) represent passes through the coastal-front boundary. The regions CD_w and CD_c refer to regions on the warm and cold sides of the front, respectively.

therm) shown in Fig. 6 emphasize the spatially inhomogeneous nature of the frontal boundary. Aircraft data for the first 8 km along the CD transect indicate relatively cooler, moister, and more turbulent flow from the east-southeast, characteristic of the cold side of the coastal front. This suggests the aircraft was flying below the front. For the next 16 km (region CD_w), the aircraft was flying in relatively warm, onshore, less turbulent flow (θ = 287 K; WD = 140°) characteristic of the warm side of the front. The remaining 25 km to point D (region CD_c) was also in the cooler, moister flow similar to the first 8 km of the CD transect. To help distinguish the location of the aircraft leg relative to the location of the coastal front, subscripts c (for cold side) and w (warm side) are used for those legs in which passes were made through the frontal boundary. Thus, CD_c is the portion of the transect from point C to D on the cold side of the coastal front.

Interestingly, the aircraft did make several passes from warmer, drier southerly flow to cooler, moister northerly flow. Transects through the frontal boundary occurred near 34.44°N, 75.76°W [regions (i) and (ii)]. The wind direction changed rapidly from southerly to northeasterly [region (i)] and then back to southerly [region (ii)]. The solid and dashed lines for the CD transect in Fig. 7 represent the passage from above the front (warm air) to below the front (cool air).

The "composite" scenario of the 12 March 1986 coastal front shown in Fig. 7 is based on low-level King Air transects, CLASS soundings, satellite pictures, and

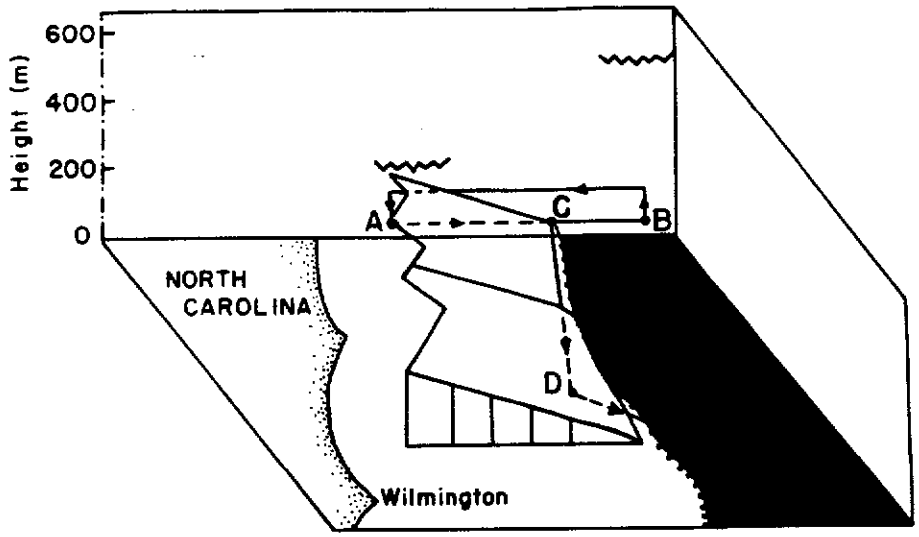

FIG. 7. Composite scenario of the 12 March 1986 coastal front valid for 2000–2200 UTC. Lines connecting *A*, *B*, *C*, *D*, and *E* represent King Air transects as given in Fig. 4. Solid lines indicate the aircraft was flying above the frontal boundary while dashed lines indicate the aircraft was under the boundary. The dotted line represents the western edge of the Gulf Stream observed to coincide with the surface position of the coastal front near *C*, but located slightly southeast of the migrated coastal front near *E*. The heavy dashed line indicates the estimated surface position of the coastal front based on a linear frontal slope.

aircraft observers' reports of cloud type and cover. The frontal location and slope given in Fig. 7 are estimated from the aircraft transects. Unfortunately, the aircraft did not make multiple passes through the front at various altitudes, so the only available estimate of the frontal slope from 30 to 148 m is a linear one (as given in Fig. 7). The estimated value of the frontal slope dz/dx using the height of the front obtained from the 30-m and 148-m transects is 3.3×10^{-3}. Thus, while the depth of the front at *C* was observed to be 30 m, the estimated height of the front at A located 50 km to the northeast is 195 m. Observations of cloud cover from the aircraft support this height. Low fractus was observed at A extending down to a height as low as 200 m, as depicted by cloud base at *A* (jagged line in Fig. 7).

If one assumes the frontal boundary is also linear from the 30-m aircraft flight level down to the ocean surface, then simple extrapolation would provide an estimate of the location of the surface position of the coastal front. The heavy dashed line over the GS shown in Fig. 7 represents this estimated location. However, from the aforementioned discussion of the relative steepness of the coastal front near the surface at *C* (and as illustrated in the traces of Fig. 5), the front appears not to extend well over the GS region, but instead is aligned more over the GS front. Indeed, this is how the coastal front is represented in the composite scenario of Fig. 7. Justification for such an alignment is provided in the aircraft transect data and SST patterns.

Consider first the transect given in Fig. 6 from *C* to region (i) where the front is intercepted by the aircraft. Because the aircraft is flying at constant altitude, estimates for the location of the surface front can only be derived from locations where the aircraft intersects the frontal boundary. Hence, for a linear frontal slope, the surface location must be exactly the same distance from the transect, and the estimated location of the surface front (dashed lines) is simply drawn parallel to the transect. In fact, if the linear frontal slope is assumed valid along the transect from *C* to region (i) at 30 m, then the transect should be precisely at the frontal boundary. In reality this is not observed because obviously the front is not a smooth, linear boundary but probably more an undulating one similar to the MABL inversion lid characterized by both cool and warm domes (Atlas et al. 1986). For the portion CD_w of the transect, because the aircraft was above the front in predominately warm onshore flow and not in the cooler offshore flow, it is reasonable to assume that the surface location of the frontal boundary was closer to the aircraft (i.e., farther northwest toward the GS front). Observations of high-resolution SST (Fig. 4) indicate that the location of the GS front was near 34.5°N, 75.5°W, or northwest of the estimated surface coastal front position. This lends credence to the assumption that the coastal front was aligned over the GS front near point *C* for the period 2000–2200 UTC.

Time series traces for the 30-m transect from *D* to *E* (not shown) indicate similar results as did the *AB* transect (Fig. 5). A sharp shift in wind direction from 20°–30° on the cool side to 160° on the warm side is

similar to that seen in the *AB* transect. Note that the surface position of the coastal front shown in Fig. 7 extends farther south from *D* as compared to *C*. This appears justified because the 30-m transect from CD_c was entirely in cool, northeasterly flow, indicating that the front was deeper from CD_c than from CD_w; that is, the surface position was farther south near *D*.

An interesting difference in the transects *DE* and *AB* is the location of the front at 30-m altitude relative to the location of the GS front. The location of the coastal front determined from the *DE* transect is not aligned over the GS front as at *C*, but the GS front appears to be located slightly farther offshore. Thus, the coastal front near *E* appears to have migrated shoreward a distance on the order of kilometers (Fig. 7). The front does not appear to be permanently tied to the GS, as also illustrated by Riordan (1990) for the GALE IOP 2 coastal front. The determination of the exact location and hence migration of the front near *E* is made more difficult by the orientation of the *DE* transect, which is more parallel to the SST gradient near the GS as compared to the nearly perpendicular *AB* transect (see Fig. 4). We consider the migration of the front in more detail in section 5.

b. *Coastal-front characteristics and the underlying SST regions*

The low-level aircraft transects given in Figs. 5 and 6 illustrate the complex relationship between the coastal front and the underlying SST regions. The transect along *AB* roughly perpendicular to the coastal front emphasizes the four distinct SST regions (Fig. 5a). The low-level atmospheric temperature and moisture structure as defined by the 30-m transect (Figs. 5c,e) indicates strong coupling of the thermodynamic field with the SST field, showing a "steplike" structure from the oceanic NS front to the MS front to the GS front. In contrast, θ and q traces for the 148-m transect show less influence of the underlying SST gradient. The transfer of heat and moisture for the more stable atmospheric conditions evident behind the coastal front (as opposed to the deeper, more well-mixed MABL over the warmer GS region) is limited to a much shallower depth. It is interesting to note the uniform θ trace over the GS at both 30 and 148 m, but a sharp decrease in moisture across the GS front.

The horizontal wind field along *AB* (as discussed in section 3a) shows a coastal front aligned over the GS front near the surface and sloping back over the MS region with the transition zone at 148 m confined between the oceanic NS and MS fronts. There is a marked deceleration of horizontal wind speed across the coastal front at 30 m (Fig. 5d), but a substantial increase in vertical velocity variance (Fig. 5f). Over the varying SST regions northwest of the GS front, there appears little coupling of SST with either wind speed or vertical velocity at 30 m. Wind speed shows an approximately linear decrease from the NS region to the GS irrespective of the SST gradient, while vertical velocity variance remains roughly constant.

The transect from *CD* (Fig. 6) aligned approximately parallel to the 20°C isotherm supports the aligning of the coastal front parallel to the GS front. The aircraft transect above the coastal front in the warm air (CD_w of Fig. 6) coincides with the region of warmest SST (Fig. 6a), as it should if the GS front (and coastal front) were located farther southeast. It is more difficult to draw conclusions concerning the coupling of the thermodynamic field with the SST field for transect *CD* (and *DE*) because of their orientation more parallel to the SST field. However, note that the coastal front must not always be strongly coupled with the underlying SST, as illustrated by the small shoreward migration of the coastal front near *E*. Also regions (i) and (ii) of Fig. 6, indicating passes through the frontal boundary, show little dependence on SST.

c. *Mean vertical structure*

Mean vertical structure in the vicinity of the coastal front on 12 March is illustrated in Figs. 8 and 9. Figure 8 shows mean vertical profiles of θ, MR, relative humidity RH, WS, and WD for the 1800 UTC 12 March CLASS soundings at Cape Hatteras, North Carolina (HAT in Fig. 4), and the leg-averaged values obtained from the over-ocean King Air stack A (2038–2102 UTC) located approximately 50 km to the southwest. This set of profiles is considered representative of the mean vertical structure in the near-coastal regions behind the coastal front from 1800 to 2100 UTC 12 March.

Typically behind an atmospheric front, the MABL is well mixed. However, the leg-averaged θ values and the 1800 UTC HAT CLASS sounding indicate a moist, stable atmosphere up to 2 km. At stack A low-level (30-m) air temperature (13.0°C) was approximately equal to the underlying SST (12.5°C) even for the cool, northeasterly MABL flow, supporting the strong stable level evident at *A*. Winds near the surface were north-northeasterly, veering almost linearly with height to southwesterly at 2 km, indicating the coastal front is indeed farther offshore.

Figure 9 shows similar soundings but for the research vessel *Cape Hatteras* (RVC in Fig. 4) at 1500, 1800, and 2100 UTC 12 March. Also given are leg-averaged values from aircraft stacks located near RVC flown at approximately the same time. The leg-averaged values given in Fig. 9a are from Electra stack EB (1449–1521 UTC). Those given in Fig. 9b are from stack EC (1606–1639 UTC), and those in Fig. 9c are from King Air stack E (2147–2231 UTC). These profile sets are considered representative of the mean vertical structure ahead of the coastal front in the warm air. The profiles indicate that RVC remained on the warm side of the coastal front from 1500 to 2100 UTC. Wind direction

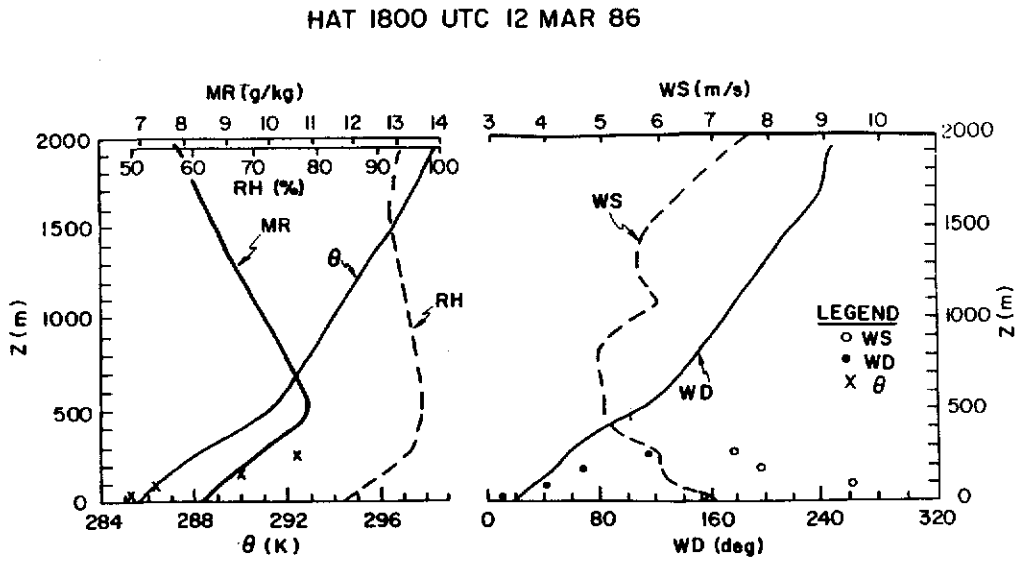

FIG. 8. The 1800 UTC 12 March 1986 CLASS sounding as shown in Fig. 3 for Cape Hatteras, North Carolina (HAT) representative of the cold side of the coastal front. Also given are leg-averaged King Air aircraft values of potential temperature, wind speed, and direction at stack A (as indicated in the legend).

in the lowest 500 m for each profile was typically onshore (90°–140°) and relatively light (3–6 m s^{-1}), as compared to the 1200 UTC RVC profile (Fig. 3), valid before the front had formed in which the wind was offshore (WD = 270°–350°). The θ profile shows a deeper, well-mixed layer as compared to behind the front. The descent (θ_1) and ascent (θ_2) profiles of potential temperature obtained from the King Air at stack E are shown in Fig. 9a. The θ observations at 1500 UTC in the lowest 500 m from the CLASS sounding, ascent and descent profiles, and leg-averaged values are all within 0.8°C. Aircraft profiles of potential temperature above 500 m differ by 1.0°–1.5°C, though the general profile shapes agree. The large descent–ascent angle of the aircraft can have a significant influence on the vertical gradients (Atlas et al. 1986) and could be responsible for the discrepancy.

The 1800 and 2100 UTC θ profiles (Figs. 9b,c) suggest a well-mixed subcloud layer of approximately 500 m. Profiles of water vapor mixing ratio indicate an increase from near the surface to approximately 500 m, supplying moisture to the overlying clouds. Observer's reports from the King Air at stack E indicated broken stratocumulus with bases near 500 m. Winds in the lowest 500 m were 2–5 m s^{-1} from the east-southeast with large shear both in magnitude and direction near cloud base. A strong, capping stable layer corresponding to cloud top was evident at a height of approximately 1750 m at 1800 UTC and had lowered to approximately 1300 m by 2100 UTC.

Stack EC is included in Fig. 9b although it is located approximately 200 km east of RVC and stacks E and EB. The relatively weak SST gradient between RVC (SST = 23°C) and EC (SST = 21°C) (Fig. 4) and the absence of any strong synoptic-scale forcing allow for reasonable comparison. The leg-averaged values of θ for EC show a well-mixed MABL similar to the 1800 UTC RVC sounding with the mean θ boundary-layer value 2°C cooler for EC than RVC—roughly the same value as the SST difference. The wind direction in the MABL is also onshore at EC as at RVC, but the wind speed magnitude at EC is approximately twice that at RVC.

4. Turbulence characteristics

a. Low-level transects

To distinguish differences in turbulence structure in the vicinity of the front, turbulence flight data from the King Air low-level transects on 12 March were divided into several legs (as emphasized in section 3 and illustrated in Fig. 7). Specifics for each leg are given in Table 2. Legs *AC*, CD_c, and DE_c were flown at a height of 30 m in the cold air west of the front, while legs *CB* and CD_w were flown at a height of 30 m, but east of the front in the warmer air. Leg *BA* is the return transect flown at a height of 148 m.

From the discussion of the sloping frontal boundary in section 3, it is apparent that knowing the location of the aircraft in relation to the location and depth of the frontal boundary is crucial to proper interpretation of turbulence statistics. For example, turbulence statistics given in Table 2 for legs *AC* and DE_c located in the cold air west of the front are within 13% of one another (with the exception of temperature variance θ'^2, which is approximately 35% smaller for leg DE_c). However, because both of these legs were flown at a

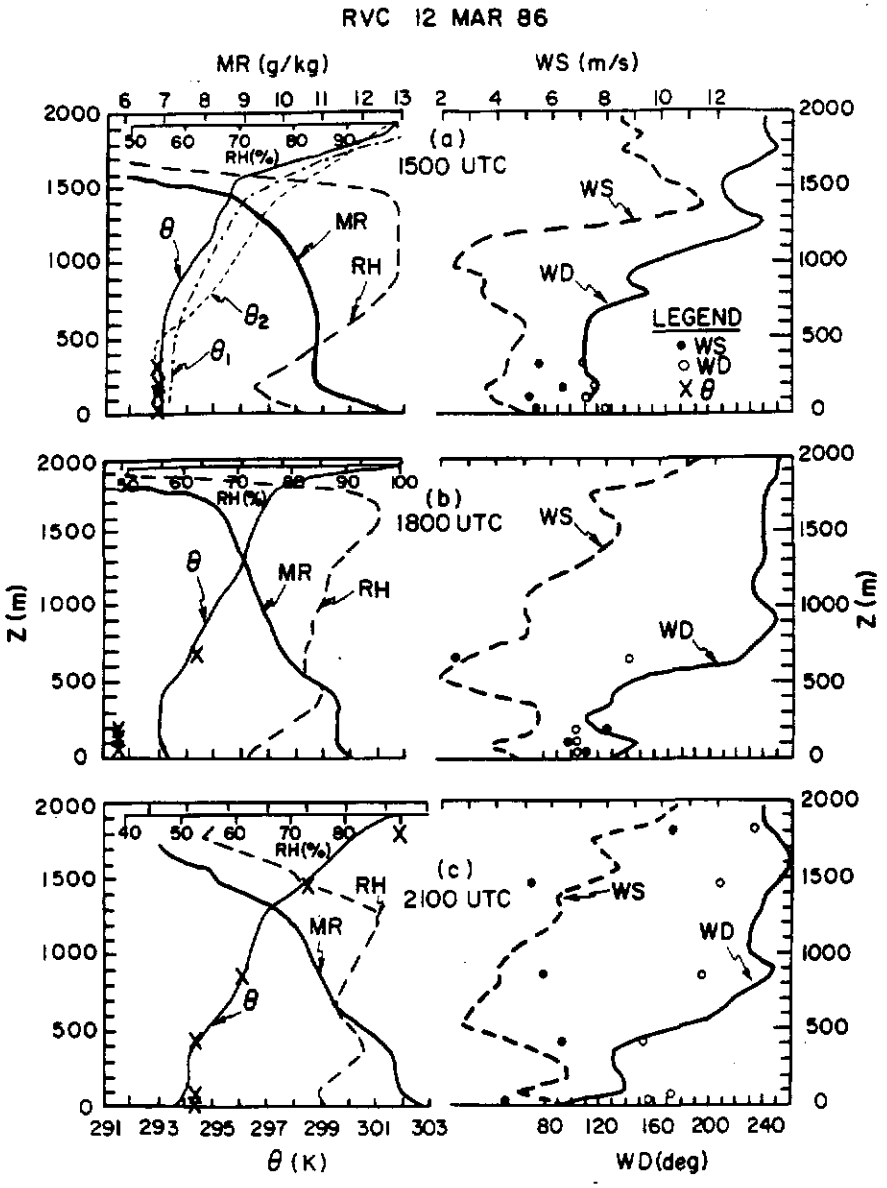

FIG. 9. The 12 March 1986 CLASS soundings at RVC as shown in Fig. 8, representative of the warm side of the coastal front for (a) 1500 UTC, (b) 1800 UTC, and (c) 2100 UTC.

constant altitude of 30 m and at a constant heading of approximately 150°, that is, approximately normal to the frontal boundary, the aircraft sampled at a normalized height (with respect to the depth of the front) that was changing with distance (as illustrated in Fig. 7). The boundary depth is less at the southeastern portion of the leg as compared to the northwestern portion. Thus, comparison of results to other legs with a constant boundary-layer depth will not be valid.

To examine the possibility of the changing depth of the front influencing turbulence at 30 m, leg AC was separated into two legs with turbulence statistics calculated for each leg (Table 3). Inherent in this examination of the effect of changing frontal depth is the need to also consider the effect of varying SST. Thus, the first leg (2002:01–2007:00 UTC) was chosen over the cooler NS waters (SST = 12°–17°C). The estimated depth of the front from the linear slope assumption would range from 195 to 121 m. The second leg (2009:46–2014:30 UTC) is the MS region located southeast of the MS front (SST = 20°C). The estimated range of frontal depth is 85 to 30 m. Thus, we would expect turbulence characteristics to differ for the two legs. We would also expect statistics over MS to agree more closely with those from leg DE_c, because of the proximity to the front and closer SST values.

TABLE 2. Variances and covariances of the perturbation quantities for 12 March King Air aircraft legs.

	Leg					
	AC	*CB*	BA_w	CD_w	CD_c	DE_c
Time (UTC)	2002:01–2014:30	2015:01–2020:00	2022:01–2031:00	2117:50–2121:00	2123:01–2128:00	2129:01–2134:00
Length (km)	56	27	41	15	25	23
Height (m)	30	30	148	30	30	30
$\overline{u'^2}$ (m s^{-1})^2	0.119	0.139	0.094	0.172	0.155	0.109
$\overline{v'^2}$ (m s^{-1})^2	0.118	0.180	0.118	0.262	0.191	0.115
$\overline{w'^2}$ (m s^{-1})^2	0.0508	0.0881	0.0782	0.0617	0.0643	0.0592
$\overline{\theta'^2}$ (°C)^2	0.0127	0.0065	0.0107	0.0051	0.0099	0.0081
$\overline{q'^2}$ (gm^{-3})^2	0.0161	0.0407	0.0130	0.0401	0.0077	0.0127
$\overline{u'w'}$ (m s^{-1})^2	0.0232	0.0196	−0.0054	0.0072	0.0012	0.0181
$\overline{v'w'}$ (m s^{-1})^2	0.0118	−0.0109	0.0044	−0.0290	−0.0339	−0.0146
$\overline{w'\theta'}$ (°C m s^{-1})	0.0065	0.0139	0.0031	0.0065	0.0016	0.0065
$\overline{w'q'}$ (g m^{-2}s^{-1})	0.0079	0.0305	0.0096	0.0181	0.0033	0.0080

Overall the statistics over MS differ only slightly from those of leg *AC* (Table 3). This simply indicates that turbulence closer to the front over warmer SST is generally larger than turbulence well behind the front over cooler SST. Similarly, turbulence values over MS agree well with leg DE_c.

Comparison of turbulence statistics over NS and MS indicates markedly different values. While there is little difference in velocity variances, moisture and temperature fluxes and variances are significantly larger closer to the frontal boundary (MS region) as compared to the NS region. Temperature ($\overline{w'\theta'}$) and moisture ($\overline{w'q'}$) fluxes and moisture variance ($\overline{q'^2}$) are three to five times larger. (The exception is temperature variance $\overline{\theta'^2}$ for NS which is influenced by the anomaly in the temperature trace of Fig. 5c near 6 km.) The increase in fluxes over MS is expected due to the increase in SST.

Leg CD_c differs from the legs in the cold air discussed previously in that it is situated roughly parallel to the front and the SST field. As discussed in section 3, the depth of the frontal boundary for leg CD_c is larger than that for CD_w. Turbulence values for leg CD_c (Table 2) are much different from those for legs MS or DE_c, but generally are within 25% of those over NS. This similarity can be seen in the time series traces of Figs. 5 and 6. This simple comparison supports the hypothesis that the front is deeper from CD_c and is probably closer in depth to that over NS.

Statistics from the three legs on the warm side of the front, *CB*, BA_w, and CD_w (Table 2), suggest a different boundary-layer regime than on the cold side. Leg *CB* east of the front at an altitude of 30 m indicates a much more turbulent boundary layer. The presence of the warmer GS is the contributing factor. Horizontal and vertical velocity variances, moisture variance, and temperature and moisture flux are significantly larger than for the 30-m legs over the cold water. Much larger fluxes of sensible heat (approximately 20 W m^{-2}) and latent heat (75 W m^{-2}) east of the front, as compared to those over the colder water, contribute to a more convective, well-mixed boundary layer.

b. *Power density spectra*

A closer examination of the scales of motion present in the vicinity of the coastal front is considered utilizing

TABLE 3. Variances and covariances of the perturbation quantities for 12 March King Air aircraft legs.

	Leg					
	AC	NS	MS	BA_{GS}	BA_{MS}	BA_{NS}
Time (UTC)	2002:01–2014:30	2002:01–2007:00	2009:46–2014:30	2022:01–2027:00	2027:01–2031:00	2032:01–2037:00
Length (km)	56	23	18	23	18	23
Height (m)	30	30	30	148	148	148
$\overline{u'^2}$ (m s^{-1})^2	0.119	0.171	0.093	0.146	0.049	0.103
$\overline{v'^2}$ (m s^{-1})^2	0.118	0.143	0.116	0.131	0.093	0.152
$\overline{w'^2}$ (m s^{-1})^2	0.0508	0.0480	0.0434	0.138	0.027	0.0341
$\overline{\theta'^2}$ (°C)^2	0.0127	0.0103	0.0097	0.0021	0.0183	0.0538
$\overline{q'^2}$ (gm^{-3})^2	0.0161	0.0047	0.0208	0.0217	0.0016	0.0195
$\overline{u'w'}$ (m s^{-1})^2	0.0232	0.0265	0.0175	−0.0075	−0.0032	−0.0117
$\overline{v'w'}$ (m s^{-1})^2	0.0118	0.0204	0.0015	0.0124	−0.0022	−0.0160
$\overline{w'\theta'}$ (°C m s^{-1})	0.0065	0.0012	0.0065	0.0049	0.0031	−0.0055
$\overline{w'q'}$ (g m^{-2}s^{-1})	0.0079	0.0027	0.0096	0.0184	0.0011	−0.0022

power spectra. Features representative of the boundary layer behind the cold front are evident in Fig. 10, which gives spectra for leg AC. Two significant peaks are evident in the horizontal velocity components u' and v' (Figs. 10a,b). Wind component u' shows a broader spectrum but one with maxima evident near the 0.1-km and 1–2-km wavelengths. Similar structure is seen in the v' component, though the peak at 2 km is much

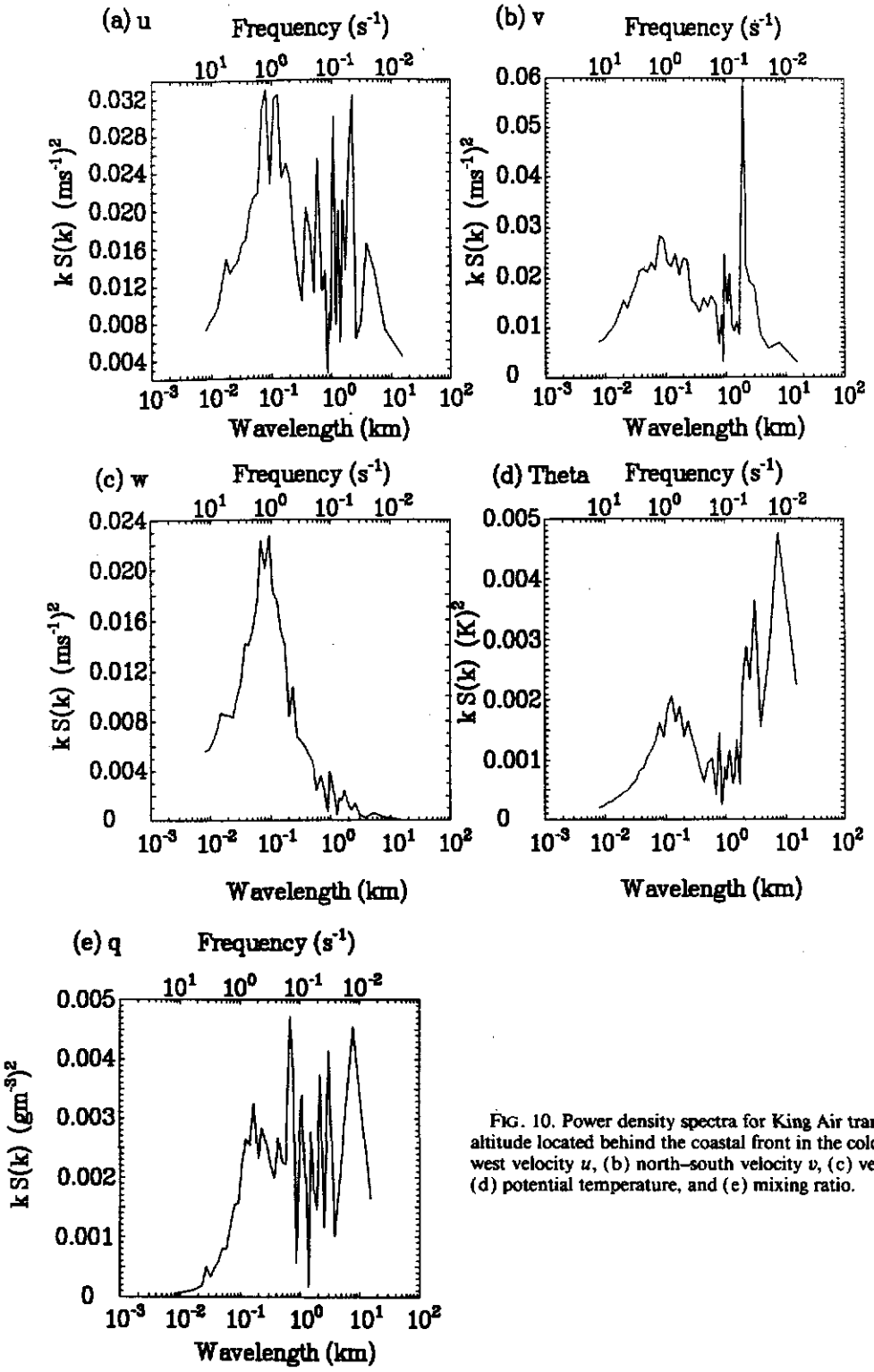

FIG. 10. Power density spectra for King Air transect AC at 30-m altitude located behind the coastal front in the cold air for (a) east–west velocity u, (b) north–south velocity v, (c) vertical velocity w, (d) potential temperature, and (e) mixing ratio.

more dominant. The peak at 1–2 km in both u' and v' is also evident in the spectra over NS and MS (not shown), indicating an organized larger-scale structure in the horizontal wind field behind the front. However, separating the NS region and the MS region and examining them individually, the 0.1-km peak is not dominant over the MS, but is the dominant wavelength over NS, suggesting smaller-scale u and v turbulence superimposed on the larger-scale flow for the cooler NS waters. Thus, over NS, while the 1–2-km wavelength is still evident (though not dominant), a larger contribution to the horizontal velocity variance is at the smaller 0.1-km wavelength. The structure of the vertical wind field for each of the legs behind the front is dominated by these wavelengths less than 0.1 km (Fig. 10c). The cospectra $u'w'$ and $v'w'$ for leg AC (Figs. 11a,b) also emphasize the importance of the 0.1-km size eddies in transferring momentum at 30-m altitude. The significant peaks in both cospectra occur near 0.1 km.

The temperature spectrum (Fig. 10d) indicates the presence of larger-scale (2–6 km) waves, which are evident both over the NS and MS regions. However, unlike the horizontal wind spectra it is these longer waves that dominate the temperature spectrum. Smaller-scale waves (0.1-km wavelength) seen in Fig. 10d are present over both the NS and MS regions.

The $w'\theta'$ cospectrum (Fig. 11c) indicates the dominant positive flux region is between the 0.03- and 0.5-km wavelength, with the peak near 0.12 km (or roughly 1.5 times the depth of the frontal boundary over MS). As seen from $\overline{w'\theta'}$ values in Table 3, it is the temperature flux over MS, not NS, that is the primary contributor to the positive heat flux. Thus, it is the smaller-scale eddies located closer to the coastal front (over the warmer oceanic MS region) that are responsible for the positive heat flux. It is the longer wavelengths that contribute to the smaller negative heat flux evident in the $w'\theta'$ cospectrum (Fig. 11c). Similar conclusions can be drawn for the moisture spectrum (Fig. 10e) and

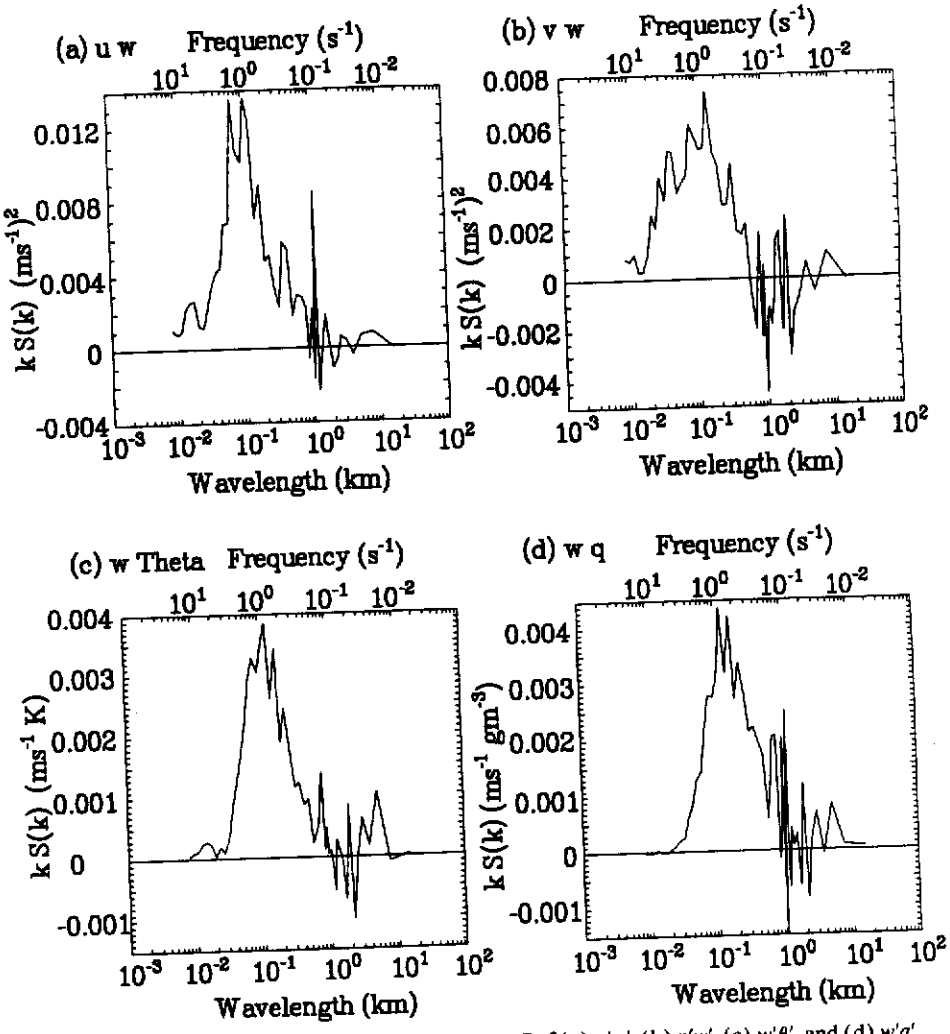

FIG. 11. Cospectral density for King Air transect AC of (a) $u'w'$, (b) $v'w'$, (c) $w'\theta'$, and (d) $w'q'$.

cospectrum (Fig. 11d). These results support the strong thermodynamic coupling evident behind the coastal front as discussed in section 3b.

Spectra obtained from leg *CB* on the warm side of the front at an altitude of 30 m (Fig. 12) differ from leg *AC* behind the front. The horizontal wind field shows a single, dominant peak wavelength of approximately 1 km (Figs. 12a,b), or approximately twice

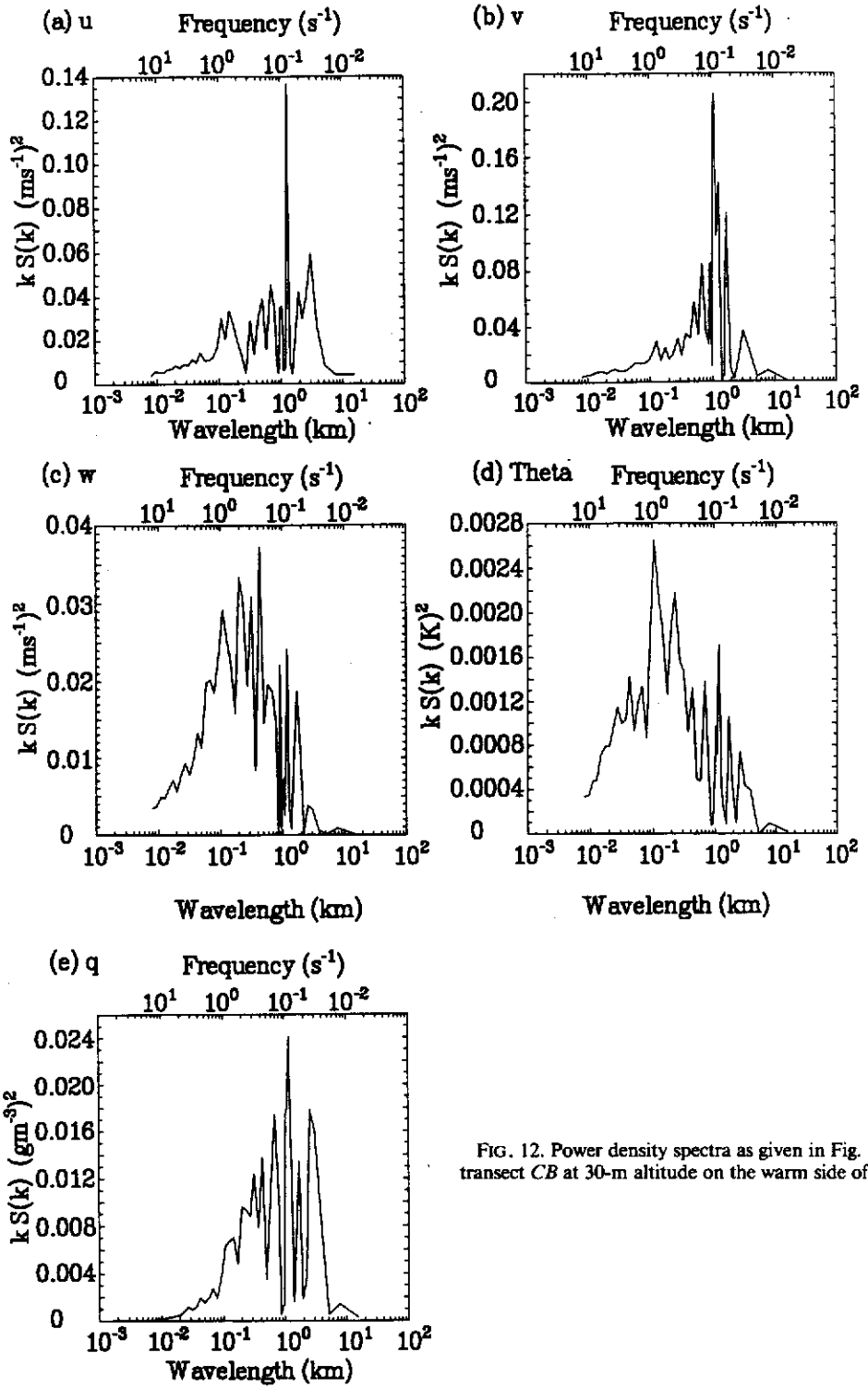

FIG. 12. Power density spectra as given in Fig. 10 for King Air transect *CB* at 30-m altitude on the warm side of the coastal front.

that of the estimated subcloud-layer depth. The vertical velocity spectrum is much broader than observed on the cold side of the front, with significant contributions to vertical velocity variance at wavelengths up to 2 km. The cospectrum of $u'w'$ (Fig. 13a) shows a similar broad spectrum, while the $v'w'$ cospectrum (Fig. 13b) has a significant peak at 1 km.

The peak wavelength in the temperature spectrum (Fig. 12d) has shifted to smaller values ($\lambda = 0.1$ km) as compared to leg AC, but still with broader, significant contributions up to the 2-km wavelength. The moisture spectrum shows a similar, rather broad spectrum with a peak centered near 1-km wavelength. The overall effect of the broader w', θ', and q' spectra is to produce rather broad cospectra for $w'\theta'$ and $w'q'$ (Figs. 13c,d). The dominant positive flux for both $w'\theta'$ and $w'q'$ is in the region between 0.1 and 2.0 km with virtually no contributions to negative flux for the entire spectra.

At an altitude of 148 m on the warm side of the front (BA_w), spectra given in Fig. 14 indicate well-defined peak wavelengths between 1 and 3 km for all variables. Horizontal wind components (Figs. 14a,b) show consistent peaks near 1–3 km similar to the structure seen at 30 m (Fig. 12). However, the peak wavelength in the vertical velocity field has shifted to larger values (0.8–1.2 km), as expected for a larger sampling altitude of 148 m. Cospectra for $u'w'$ and $v'w'$ shown in Figs. 15a,b also support the dominant 1–3-km-size eddies.

The temperature and moisture fields (Figs. 14d,e) show dominant peaks at longer wavelengths, but without the contributions at smaller wavelengths from 0.1 to 0.5 km evident at 30-m altitude (Fig. 12). The relatively small positive flux (0.0031°C m s^{-1} in Table 3) for the $w'\theta'$ cospectrum is a result of the approximate balance of the positive flux from wavelengths near 1 km and the negative flux of longer wavelengths between 2 and 4 km (Fig. 15c). This contrasts the broad spectrum of positive heat flux seen at 30 m (Fig. 12). The $w'q'$ cospectrum (Fig. 15d) shows similar features to the $w'\theta'$ cospectrum for $\lambda < 2$ km. However, a signif-

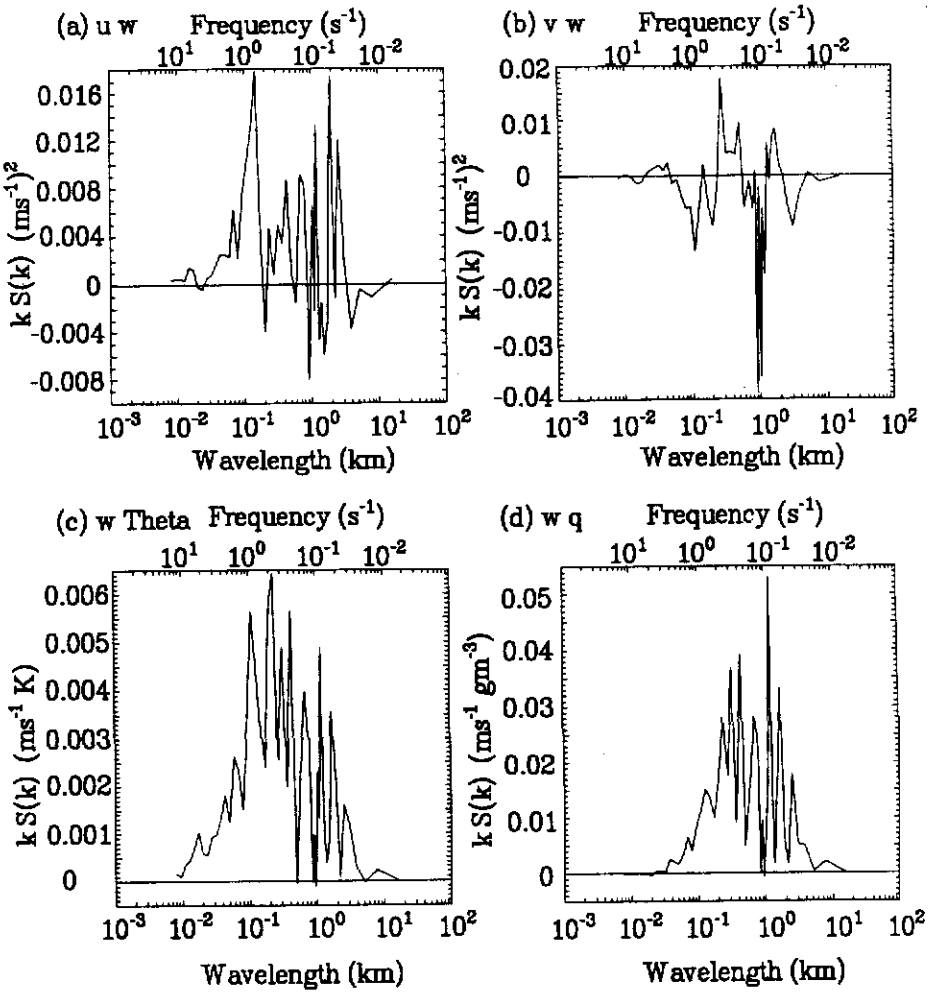

FIG. 13. Cospectral density as given in Fig. 11 for King Air transect CB.

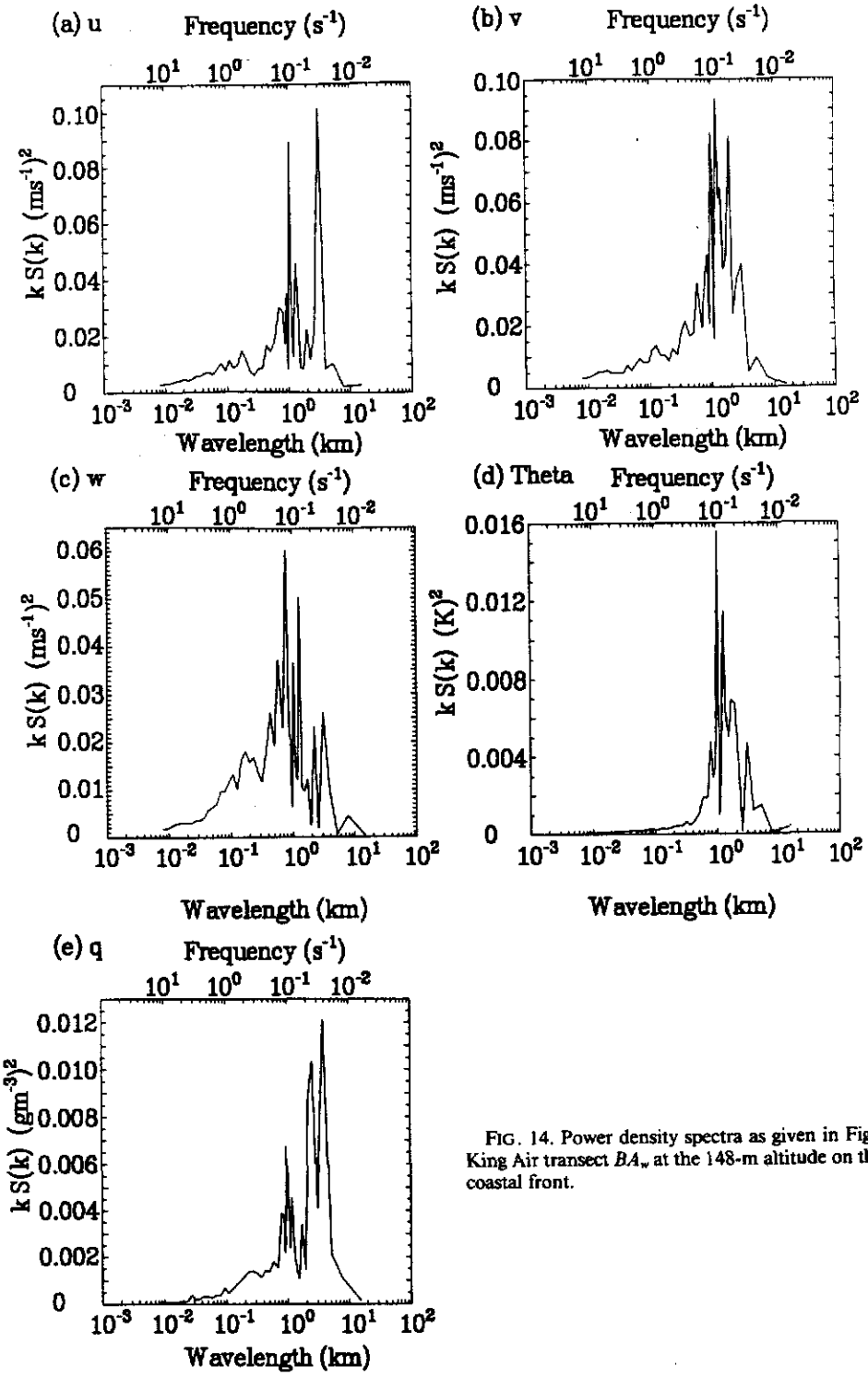

FIG. 14. Power density spectra as given in Fig. 10 for the return King Air transect BA_w at the 148-m altitude on the warm side of the coastal front.

icant difference for $\lambda > 2$ km is the large positive flux contribution for wavelengths on the order of 2–4 km, a region of significant negative temperature flux.

c. *MABL structure above the frontal boundary*

Closer examination of the time series traces above the frontal boundary is considered to investigate the presence of an organized atmospheric wave structure. We consider here the *BA* transect to examine the influence of the frontal boundary on MABL structure. (Similar conclusions can be drawn from transect CD_w also located above the coastal-front boundary in the warm air.) Production of waves by penetrating thermals into the overlying stable region has been studied in

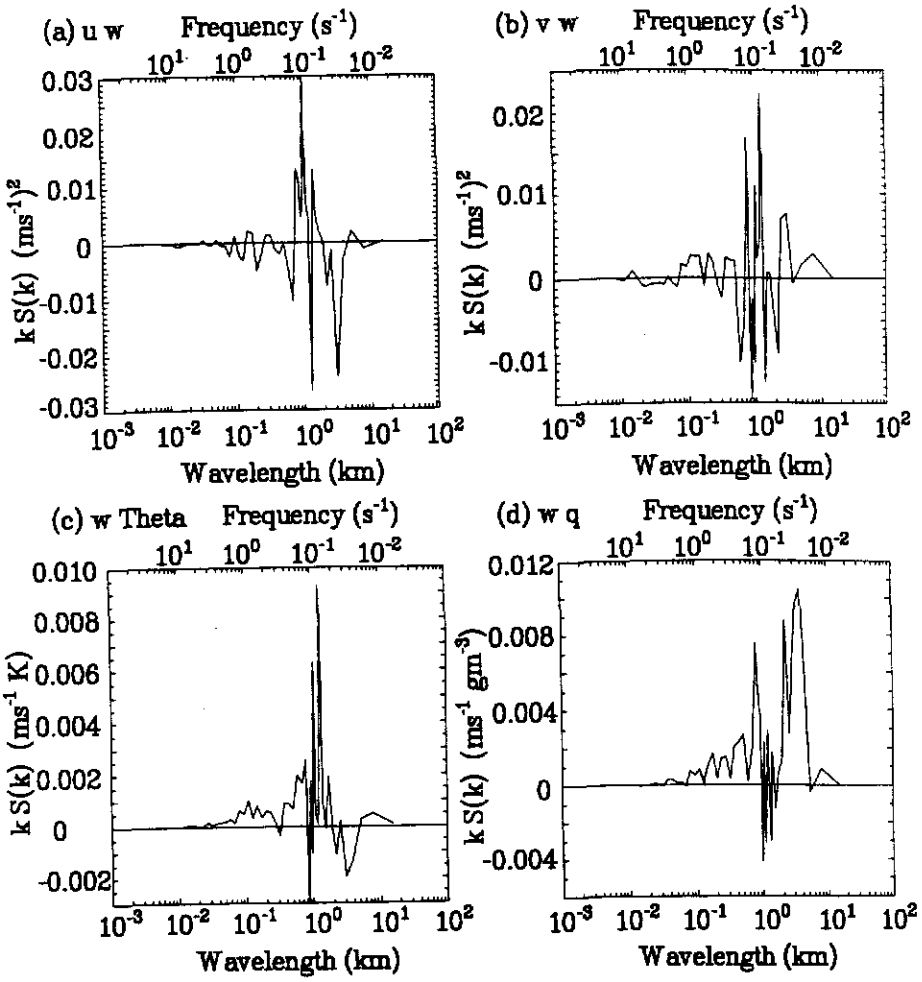

FIG. 15. Cospectral density as given in Fig. 11 for King Air transect BA_w.

both laboratory tanks and numerical simulations. Numerical simulations of Gall et al. (1988) emphasized the presence and generation mechanisms for gravity waves produced during frontogenesis. They proposed that these waves were generated by imbalances in the frontal zone not dissimilar to mountain waves. However, no documentation in the literature for the presence of waves along a shallow coastal front has been provided.

Figure 16 shows time series traces for a 60-s portion of transect BA_w at 148 m. The traces shown are over the MS region of Fig. 5 from approximately 40 to 45 km. Also given in Fig. 16 is a plot of the indicator function that is used to define updraft and downdraft events as outlined by Greenhut and Khalsa (1987) (see section 4d). Simply stated, a threshold for updrafts (or downdrafts) is defined as the square root of one-half the variance of all positive (or negative) fluctuations of w about $w = 0$. If vertical velocity fluctuations are greater than the threshold value, then the indicator function is assigned a value of +1 (or −1). Otherwise the indicator function is assigned a value of zero (or environment). A minimum event time of 0.4 s (or 8 points at 20 samples per second) is required. This corresponds to a minimum event length of approximately 30 m, which is well below the dominant scale of flux-producing events (Mahrt and Paumier 1984).

The traces of vertical velocity, temperature T, and mixing-ratio fluctuations given in Fig. 16 suggest the presence of wave activity. It is well known that buoyancy waves characteristically show temperature fluctuations 90° out of phase with vertical velocity fluctuations. Correlation analysis of w' and T' indicates large correlation for a spatial lag of 210 m, indicating a dominant wavelength of approximately 840 m. The indicator function also points to a wavelength on the order of 1 km. These results agree with those of the spectral analysis presented in Fig. 14 for leg BA_w.

It is hypothesized here that the presence of these buoyancy waves is due to the influence of the underlying coastal front in generating instabilities, which propagate out from the boundary. Evidence to support this hypothesis is given in the cospectral plots of Fig. 17. Shown are the $w'\theta'$ cospectra for three regions of

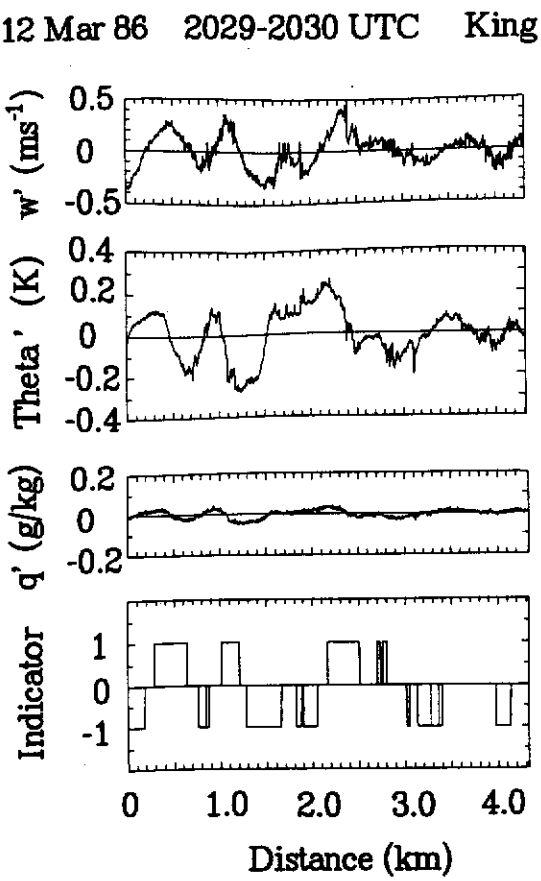

FIG. 16. King Air time series trace at the 148-m altitude from 2029 to 2030 UTC 12 March over the oceanic midshelf region on the warm side of the coastal front (BA_w) of (a) vertical velocity, (b) temperature, (c) mixing ratio, and (d) indicator function.

the 148-m return transect from B to A. The first two legs, designated BA_{GS} and BA_{MS} (as detailed in Table 3), were located on the warm side of the front but over the GS and MS regions, respectively. The third leg BA_{NS} was located over the NS region in the cold air beneath the coastal front.

The cospectra indicate that over the GS (Fig. 17a), eddies on the scale of 0.1–1.0 km contribute to the cospectral energy, similar to Fig. 15c. This is an indication of the wider range of scales of motion present in the well-mixed MABL over the GS, up to approximately twice the depth of the MABL. From the discussion of Fig. 12 for transect CB at 30 m, this broader range of eddies contributing to heat flux ranging from 0.1 to 1.0 km was also evident. This contrasts the cospectra given in Fig. 17b for the MS region located above the frontal boundary. Here the contribution to cospectral energy in the 0.1–0.5-km range is greatly reduced, indicating the absence of these smaller-scale eddies. It is the presence of the coastal front that inhibits the generation of these eddies. As over the GS, the dominant 1-km wave is still present. The cospectrum for transect BA_{NS} (Fig. 17c) located beneath the coastal front shows the dominant 1.0–1.5-km wavelength that contributes to a sink of cospectral energy.

d. Conditional sampling statistics

Conditional sampling techniques can be used to investigate variations in turbulence structure in the vicinity of the front. Such techniques have been employed previously (e.g., Grossman 1984; Greenhut and Khalsa 1987; Rogers 1989) to study subcloud-layer convection. The bivariate conditional sampling technique as proposed by Holland (1973) is used here. Holland showed that the vertical flux of a passive scalar, such as virtual potential temperature θ_v, can be divided into four components

$$\overline{w'\theta'_v} = \underbrace{\overline{w'_+\theta'_{v+}}}_{\text{PP}} + \underbrace{\overline{w'_+\theta'_{v-}}}_{\text{NP}} + \underbrace{\overline{w'_-\theta'_{v-}}}_{\text{PN}} + \underbrace{\overline{w'_-\theta'_{v+}}}_{\text{NN}} \quad (2)$$

where, for example, PN designates a positive flux (P)($\overline{w'\theta'_v} > 0$) associated with a negative vertical velocity (N). Thus, thermally direct motions are given as PP (rising, positively buoyant air) and PN (sinking, negatively buoyant air). Thermally indirect motions are designated as NP and NN. Small-scale mixing associated with entrainment and detrainment is typically of smaller magnitude, though still important in subcloud-layer and cloud-top dynamics, as compared to direct motions.

Table 4 summarizes the results of the mean partitioned buoyancy fluxes for the 12 March 1986 aircraft legs. Table 4a gives the mean fluxes for each individual leg while Table 4b gives the mean fluxes for a specific height (30 or 148 m) and region with respect to the coastal front.

Fluxes over the warmer GS region (leg CB) show the largest total buoyancy flux as expected. The primary contributor to the total flux is warm updrafts (PP); however, cool downdrafts (PN) do make a significant contribution. In fact, the majority of time for leg CB (41%) is characterized as PN. Thus, while it is the intense, narrower warm updrafts that dominate the total flux, it is the broader, less intense cool downdrafts that occupy a larger portion of the transect over the GS.

Fluxes at 30 m above the frontal boundary in the warm air (leg CD_w) show a 55% reduction in total flux compared to over the GS. The percentage of area occupied by each partitioned flux is approximately equal, except for the flux NN, which is larger for CD_w over the frontal boundary than over the GS. This indicates the presence of entraining eddies just above the front not seen over the GS.

Table 4a emphasizes that the bulk of the total flux for the region from NS to the GS (leg AC) is due to the MS region as opposed to the NS region. Leg DE_c is similar to AC in flux magnitudes as well as percentages, indicating that a majority of time is spent in PP and PN modes.

To understand the importance of the frontal boundary in affecting the distribution of fluxes, the partitioned

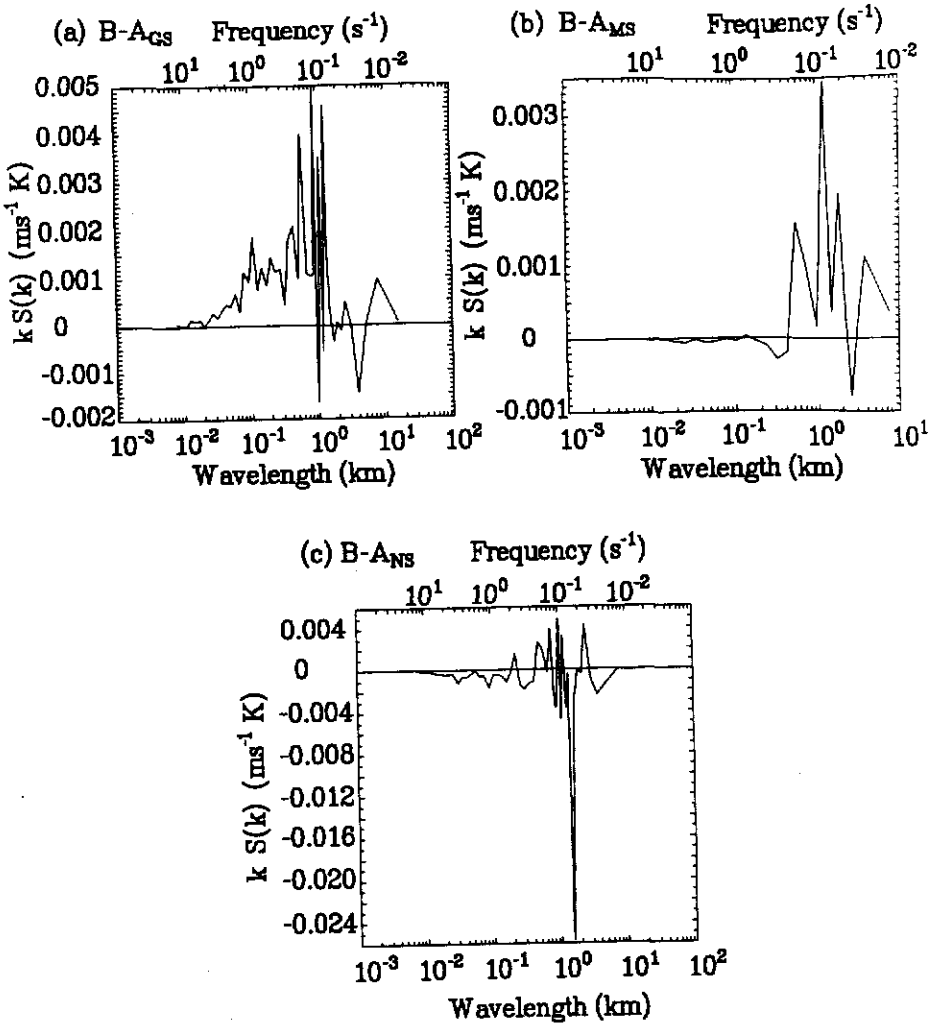

FIG. 17. Cospectral density $w'\theta'$ for three regions of the 148-m *BA* transect: (a) BA_{GS} located over the Gulf Stream, (b) BA_{MS} located over the midshelf region, and (c) BA_{NS} located over the nearshore region. The Gulf Stream and midshelf regions were located on the warm side of the front while the nearshore region was located beneath the front on the cold side.

fluxes were averaged with respect to altitude and location (Table 4b). The values given are averages for all 12 March low-level King Air aircraft legs. For the averaged fluxes at 30 m on the cold versus the warm side of the front, there is surprisingly little difference in the magnitude of warm updrafts (PP). We would expect the warmer SST region to have a larger contribution from PP. The reason that warm updrafts are smaller than expected is because the averaged flux at 30 m (warm) represents aircraft transects from *CB* over the GS (where we would expect PP to be large), in addition to transects above the coastal-front boundary (where PP is inhibited by the coastal-front boundary). The major difference for the warm and cold sides at 30 m occurs for fluxes PN and NN. The warm side is characterized by broader, cooler downdrafts (PN) while the cold side generally has a larger contribution from warmer downdrafts (NN).

In the cold air at 30 m, direct fluxes accounted for an average of 56% of the total time with 44% due to indirect fluxes. On the warm side at 30 m, direct fluxes occurred 68% of the time and indirect 32%. These results compare favorably with the estimates of Rogers (1989), obtained across an oceanic SST front during FASINEX, and Grossman (1984) over the Atlantic trade winds near Barbados. Over the warmer water Rogers reported average times of 62% and 38% in direct and indirect modes, respectively, while Grossman indicated 64% and 36%. Rogers showed values of 54% and 46% in direct and indirect modes over the colder water.

At 148 m, the major difference for the cold and warm sides is the magnitude and direction of the total flux. The 148-m cold region is the region located just beneath the coastal front near stack A (Fig. 7). The total flux is negative (as seen in the cospectrum of Fig. 17c), but

TABLE 4a. Mean partitioned buoyancy fluxes (10^3 K m s^{-1}) for 12 March 1986 for each aircraft leg. The percentage of area occupied by each partition is given in parentheses.

Leg	PP	NP	PN	NN	Total
AC	7.22 (26)	−2.44 (20)	4.80 (30)	−3.01 (24)	6.57
CB	10.32 (28)	−1.29 (18)	5.47 (41)	−1.11 (13)	13.39
BA_w	4.79 (28)	−2.39 (21)	3.72 (27)	−2.30 (24)	3.82
CD_w	5.16 (29)	−0.97 (19)	3.54 (35)	−1.52 (17)	6.21
CD_c	5.75 (27)	−2.23 (24)	3.29 (27)	−5.10 (22)	1.71
DE_c	7.51 (30)	−1.71 (21)	3.29 (27)	−2.71 (22)	6.38
NS	4.16 (24)	−2.51 (25)	3.43 (27)	−3.84 (24)	1.24
MS	6.52 (28)	−1.57 (17)	3.95 (28)	−2.27 (27)	6.63

not due entirely to entrainment (NN). A significant portion of the negative flux is due to rising, cooler air (NP). In fact, NP occupies more area than NN and is suggestive of an indirect circulation. The 148-m cold-air region shows the lowest percentage of time occupied in the direct mode (50%) of the four regions.

5. Discussion and conclusions

Examination of the low-level atmospheric structure of a coastal front in the vicinity of SST discontinuities for the 12 March 1986 GALE case offshore of the Carolinas illustrates the complex interaction of the oceanic and atmospheric fronts. The 12 March coastal front is observed to be a shallow (less than 200 m), highly spatial inhomogeneous surface, that is, at times closely thermodynamically coupled with the underlying SST. Behind the front in the cold air, the atmosphere can be generally characterized as moister and more statically stable than ahead of the front in the warm air. Two distinctly different oceanic regions that are also characterized by different atmospheric thermodynamic structure are evident behind the coastal front. Over the MS oceanic region, turbulent eddies on the scale of 1.5 times the depth of the front (120 m) are solely responsible for the positive heat flux. Within the NSS, located between the NS and MS regions, the transition zone of the coastal front aloft is confined. Over the NS waters, a smaller air–sea temperature difference that effectively limits the magnitude of temperature perturbations results in much smaller production of heat flux from warm updrafts. The horizontal wind structure of this NS region is dominated more so by smaller-scale waves (100-m wavelength) superimposed on a weaker, longer scale (1–2 km) wave structure.

The deeper (approximately 500–600 m), more well-mixed subcloud layer (broken cumulus and stratocumulus) ahead of the front is characterized by a dominant scale of turbulent eddies on the order of 1 to 2 km. Conditional sampling emphasizes the strong direct circulation established over the GS dominated by intense, narrow, warm updrafts and broader, less intense cool downdrafts. In contrast, the cooler, fractus-topped and layered, stratocumulus-topped region behind the coastal front is characterized by an indirect circulation with more prevalent cool updrafts and warm downdrafts, particularly for the near–cloud-base region (148 m). Friehe et al. (1991) also showed that the negative sensible heat flux near cloud base for a similar case of air flowing from cold water to warm during FASINEX was a result of cool updrafts.

Thus, the presence of differing SST regions strongly influences the thermodynamic structure of the marine atmospheric boundary layer (MABL). However, the coupling between the MABL and the underlying SST fields is not a simple cause and effect relationship. Aircraft observations indicate regions exist on 12 March in which the location of the GS front and the atmospheric coastal front coincide almost exactly. Sharp horizontal gradients of atmospheric temperature, moisture, wind speed, and direction are aligned with the GS SST gradient. But regions also exist in which the two fronts do not coincide. Thus, the front does not always appear to be dynamically tied to the underlying surface.

The migration of coastal fronts onshore has been addressed by Riordan (1990) and Nielsen (1989). Riordan showed that it is the combined effect of low-level confluence and differential diabatic heating (due primarily to the underlying SST gradient) that promoted the onshore movement of a coastal front in the GS region during GALE. The confluence served to reinforce the low-level thermal gradient just west (or shoreward) of the coastal front. He also noted that the fixed confluent axis shoreward of the coastal front was evident during the nighttime hours only. It is interesting to note that the coupling of the atmospheric and oceanic fronts for this study was valid for the time period 2000–2200 UTC (late afternoon local time). The premise is that the coastal front is sensitive to regions of differential surface heating and cooling. During the day, the significant contrast of low-level warming of the MABL over the GS versus the reduced warming over the NS and MS waters helps to establish a ther-

TABLE 4b. Mean partitioned buoyancy fluxes (10^3 K m s^{-1}) for 12 March 1986 averaged by altitude and location. The percentage of area occupied by each partition is given in parentheses.

Location	PP	NP	PN	NN	Total	Direct (%)
30 m, cold	6.83 (27)	−2.13 (21)	3.79 (29)	−3.61 (23)	4.88	56
30 m, warm	7.74 (29)	−1.13 (18)	4.51 (39)	−1.32 (14)	9.80	68
148 m, cold	5.45 (23)	−8.50 (27)	6.29 (27)	−8.62 (23)	−5.38	50
148 m, warm	4.79 (28)	−2.39 (21)	3.72 (27)	−2.30 (24)	3.82	55

mally direct circulation. However, a more significant land–sea temperature difference evident nearer the coast later at night may provide the coastal front a more conducive environment for development, thus promoting the movement or migration onshore.

For the present study, examination of the low-level wind field may give some insight into the movement of the front. The slight deceleration of horizontal wind speed observed across the front at 30 m from transect *AB* (Fig. 5d) is a result of a small frontally induced pressure gradient, as also emphasized by Wai and Stage (1989) in a numerical study of the GS front. They demonstrated that upwind of the SST front in the cold air, the perturbation pressure gradient force acts to accelerate the low-level flow. Downwind the flow is similarly decelerated. The horizontal extent of their simulated SST front, and thus the magnitudes of wind speed and acceleration, differ from this study, but the reasoning is still valid.

The importance of the low-level wind field in the movement of the coastal front was shown by Nielsen (1989). He examined certain New England coastal fronts as examples of quasi-stationary density currents and emphasized that stronger onshore flow in relation to surface heating, as in sea-breeze dynamics, can influence the onshore movement of the front. Pertaining to the movement of the 12 March coastal front shoreward, note that relatively weak (2 m s^{-1}) southerly flow was present just ahead of the front along transect *CB*. In contrast, just ahead of the front farther to the southwest along transect *DE*, stronger (5 m s^{-1}) southerly flow was present. Remember that the surface location of the coastal front along *DE* was slightly shoreward of the GS front. The presence of stronger onshore flow would support the shoreward migration.

While the migration of the coast front is important, it is not the focus of this study. Knowledge of the location of the front, whether it is aligned or coupled with specific SST regions, is interrelated with the movement of the front. But from this study of the dynamics of the 12 March GALE coastal front, we have emphasized that the coastal front has a significant effect on the 3D atmospheric circulation. The two most obvious effects of the frontal boundary on MABL circulation are the thermodynamic decoupling of the region above the frontal surface from that below the surface and the influence of the frontal boundary on the generation of buoyancy waves above the front. The premise of a front as a material surface that effectively inhibits the transfer of properties across the boundary has been proposed by many (see Wallace and Hobbs 1977). Aircraft observations on 12 March indicate that while the coastal front is indeed a spatially inhomogeneous, undulating surface in which convective thermals can penetrate, the front can severely limit the transfer of heat and moisture fluxes to the atmosphere above the front. This is achieved primarily through the damping of smaller turbulent eddies on the scale of the depth of the front (100 m). This damping is confined to regions above the front, and particularly concentrated in the MS region. Over the warmer GS, strong vertical mixing over the depth of the MABL occurs. Unfortunately, direct observations of the strength of the inversion in the MS region were not available to assess the ability to suppress transport across the frontal boundary.

In conjunction with the decoupling over the MS region, the presence of the frontal boundary is also observed to be a source of buoyancy waves. The importance of the waves is that they can act to deplete kinetic energy and momentum from the environment as they vertically and horizontally propagate. The subsequent stabilization of the region above the frontal surface due to the decrease in the vertical transfer of fluxes from the surface provides favorable conditions for wave formation. Estimates of the Monin–Obukhov length L (Lumley and Panofsky 1964) from 30-m aircraft data indicate more near-neutral stability for legs CD_w ($L = -37$ m) above the frontal boundary, as compared to the more convective GS leg *CB* ($L = -13$ m). It is observed that turbulence immediately above the frontal surface is generally reduced as compared to that below the surface (see vertical-velocity trace from CD_w in Fig. 6). Subsequently, instabilities present along the frontal surface can serve as the trigger for these waves.

Finally, we should mention the mechanisms responsible for the formation of the 12 March coastal front. The mechanisms bear resemblance to those of a simple internal boundary layer (IBL) that develops due to step changes in surface temperature or roughness. Numerical model results of Taylor (1971) and more recently Koracin and Rogers (1990) have shown that a stable IBL can develop for airflow from the warm side of a SST front to the cold side. A minimum in surface stress is associated with the IBL, with a corresponding decrease in wind speed within the IBL. Observational results from FASINEX (Friehe et al. 1991) show a 50% decrease in momentum flux as air flows from warm to cold water. Statistics given in Tables 2 and 3 for the 12 March coastal front do not show a large change in momentum flux across the front. Values of friction velocity show only small changes (0.13–0.18 m s^{-1}). The formation of the coastal front does not appear to be due solely to changes in the surface fluxes. The winds are typically light on both sides of the front, and the slight change in wind speed across the front does not produce significant changes in surface drag. This is only one study, and more studies of coastal fronts under different wind regimes are needed to better understand the interaction of the coastal front and the SST front.

Our examination of this interaction has demonstrated the impact of underlying SST discontinuities on the 3D atmospheric boundary-layer circulation. The coastal front itself is of meteorological significance because it serves as a focal point for physical processes such as low-level flux convergence and differential diabatic heating that are known to directly affect cyclo-

genesis. Future research should thus seek to further validate the atmospheric structure and important physical processes in an attempt to better understand the interaction of the coastal front and ensuing cyclogenesis.

Acknowledgments. This work was prepared in conjunction with research funded by the Naval Postgraduate School Research Initiation Fund and by the Division of Atmospheric Sciences, National Science Foundation, under Grant ATM-88-01650. Special thanks to an anonymous reviewer for helpful suggestions in the revision of the manuscript, and to LuAnn Salzillo for expert drafting of the figures.

REFERENCES

Atlas, D., B. Walter, S.-H. Chou, and P. J. Sheu, 1986: The structure of the unstable marine boundary layer viewed by lidar and aircraft observations. *J. Atmos. Sci.*, **43**, 1301–1318.

Ballentine, R. J., 1980: A numerical investigation of New England coastal frontogenesis. *Mon. Wea. Rev.*, **108**, 1479–1497.

Bosart, L. F., 1975: New England coastal frontogenesis. *Quart. J. Roy. Meteor. Soc.*, **101**, 957–978.

——, and S. C. Lin, 1984: A diagnostic analysis of the Presidents' Day Storm of February 1979. *Mon. Wea. Rev.*, **112**, 2148–2177.

Carson, R. B., 1950: The Gulf Stream front: A cause of stratus on the lower Atlantic coast. *Mon. Wea. Rev.*, **78**, 91–101.

Friehe, C. A., W. J. Shaw, D. P. Rogers, K. L. Davidson, W. G. Large, S. A. Stage, G. H. Crescenti, S. J. S. Khalsa, G. K. Greenhut, and F. Li, 1991: Air–sea fluxes and surface-layer turbulence around a sea surface temperature front. *J. Geophys. Res.-Oceans*, **96**, 8593–8609.

Gall, R. L., R. T. Williams, and T. L. Clark, 1988: Gravity waves generated during frontogenesis. *J. Atmos. Sci.*, **45**, 2204–2219.

Greenhut, G. K., and S. J. S. Khalsa, 1987: Convective elements in the marine atmospheric boundary layer. Part I: Conditional sampling statistics. *J. Climate Appl. Meteor.*, **26**, 813–822.

Grossman, R. L., 1984: Bivariate conditional sampling of moisture flux over a tropical ocean. *J. Atmos. Sci.*, **41**, 3228–3253.

Herbster, C. G., 1990: The vertical structure of the marine atmospheric boundary layer across a sea surface temperature front. M.S. thesis, Department of Meteorology, Florida State University, 164 pp. [Available from Dept. of Meteorology, Florida State University, Tallahassee, FL 32306-3034.]

Holland, J. Z., 1973: A statistical method for analyzing wave shapes and phase relationships of fluctuating geophysical variables. *J. Phys. Oceanogr.*, **3**, 139–155.

Khalsa, S. J. S., and G. K. Greenhut, 1989: Atmospheric turbulence structure in the vicinity of an oceanic front. *J. Geophys. Res.*, **94**, 4913–4922.

Kocin, P. J., and L. W. Uccellini, 1984: A review of major East Coast snowstorms. Preprints, *10th Conf. on Weather Forecasting and Analysis*, Clearwater Beach, FL., Amer. Meteor. Soc., 189–198.

Koracin, D., and D. P. Rogers, 1990: Numerical simulations of the response of the marine atmosphere to ocean forcing. *J. Atmos. Sci.*, **47**, 592–611.

LeMone, M. A., and W. T. Pennell, 1980: A comparison of turbulence measurements from aircraft. *J. Appl. Meteor.*, **19**, 1420–1437.

Lenschow, D. H., and P. Spyers-Duran, 1986: Measurement techniques: Air motion sensing. NCAR Bulletin No. 23, 47 pp. [Available from NCAR, Boulder, CO 80307.]

Lind, R. J., and W. J. Shaw, 1991: The time-varying calibration of an airborne Lyman-α hygrometer. *J. Atmos. Oceanic Technol.*, **8**, 186–190.

Liu, W. T., and K. B. Katsaros, 1984: Spatial variation of sea surface temperature and flux-related parameters measured from aircraft in the JASIN experiment. *J. Geophys. Res.*, **89**, 10 641–10 644.

Lumley, J. L., and H. A. Panofsky, 1964: *The Structure of Atmospheric Turbulence.* J. Wiley Interscience, 239 pp.

Mahrt, L., and J. Paumier, 1984: Heat transport in the atmospheric boundary layer. *J. Atmos. Sci.*, **41**, 3061–3075.

Marks, F. D., Jr., and P. M. Austin, 1979: Effects of the New England coastal front on the distribution of precipitation. *Mon. Wea. Rev.*, **107**, 53–67.

Nielsen, J. W., 1989: The formation of New England coastal fronts. *Mon. Wea. Rev.*, **117**, 1380–1401.

——, and P. P. Neilley, 1990: The vertical structure of New England coastal fronts. *Mon. Wea. Rev.*, **118**, 1793–1807.

Raman, S., and A. J. Riordan, 1988: The Genesis of Atlantic Lows Experiment: The planetary boundary-layer subprogram of GALE. *Bull. Amer. Meteor. Soc.*, **69**, 161–172.

Riordan, A. J., 1990: Examination of the mesoscale features of the GALE coastal front of 24–25 January 1986. *Mon. Wea. Rev.*, **118**, 258–282.

Rogers, D. P., 1989: The marine boundary layer in the vicinity of an ocean front. *J. Atmos. Sci.*, **46**, 2044–2062.

Taylor, P. A., 1971: Airflow above changes in surface heat flux, temperature and roughness; an extension to the stable case. *Bound.-Layer Meteor.*, **1**, 474–507.

Wai, M. M., and S. A. Stage, 1989: Dynamical analyses of marine atmospheric boundary layer structure near the Gulf Stream oceanic front. *Quart. J. Roy. Meteor. Soc.*, **115**, 29–44.

Wallace, J. M., and P. V. Hobbs, 1977: *Atmospheric Science.* Academic Press, 467 pp.

Warner, T. T., M. N. Lakhtakia, J. D. Doyle, and R. A. Pearson, 1990: Marine atmospheric boundary layer circulations forced by Gulf Stream sea surface temperature gradients. *Mon. Wea. Rev.*, **118**, 309–323.